CHAPTER V

METHANOL SYNTHESIS WITHOUT SLURRY CIRCULATION

5.1 Introduction

Liquid-entrained operations at the LaPorte liquid phase methanol process development unit continued with a simplified and optimized process(Air Products 1992). The process with circulation of slurry described in previous chapter was no longer in use since costly operation. A series of operations RUN E-8 was conducted in a process without circulation of slurry. This chapter described the simulations for the case RUN E-8.1 (Gidaspow et al. 1995). An internal heat exchanger was considered in this computation and kinetic theory approach is used to compute the solid viscosity.

In order to examine the convergence of the computational techniques, an additional simulation run was made with same operating conditions except of the grid size.

5.2 Reaction and Kinetics Model

To predict a more accurate methanol production rate, a power law rate expression, depicted in Air Products' (1992) report, is used in this computational run. The model was based on the rate expressions for methanol synthesis (Weimer et al. 1987) and the parameters were determined from experimental research.

$$r=\varepsilon_s\rho_s K_r f_{co}^{1/3} f_{H_2}^{2/3}\left(1-\frac{f_{MEOH}}{K_{eq} f_{co} f_{H_2}^2}\right)$$

The mass transfer and species balances are same as that described in chapter 4.

5.3 Mathematical Models (Kinetic Theory)

Energy equation is needed in this simulation because of non-isothermal situation with internal heat exchanger. The kinetic theory approach is used for computing the solid pressure and viscosity.

5.3.1 Continuity Equations

Gas Phase:

$$\frac{\partial}{\partial t}(\varepsilon_g \rho_g)+\nabla\cdot(\varepsilon_g \rho_g \mathbf{v}_g)=\dot{m}_g$$

Liquid and Solid Phase: ($k=\ell,s$)

$$\frac{\partial}{\partial t}(\varepsilon_k \rho_k)+\nabla\cdot(\varepsilon_k \rho_k \mathbf{v}_k)=\dot{m}_k$$

5.3.2 Momentum Equations

Gas Phase:

$$\frac{\partial}{\partial t}(\varepsilon_g \rho_g \mathbf{v}_g)+\nabla\cdot(\varepsilon_g \rho_g \mathbf{v}_g \mathbf{v}_g)=\varepsilon_g \rho_g \mathbf{F}_g+\sum_{m=\ell,s}\beta_{gm}(\mathbf{v}_m-\mathbf{v}_g)+\nabla\cdot[\tau_g]+\dot{m}_g \mathbf{v}_g$$

Liquid and Solid Phase: ($k=\ell,s$)

$$\frac{\partial}{\partial t}(\varepsilon_k \rho_k \mathbf{v}_k)+\nabla\cdot(\varepsilon_k \rho_k \mathbf{v}_k \mathbf{v}_k)=\varepsilon_k \rho_k \mathbf{F}_k+\sum_{m=g,\ell,s}\beta_{km}(\mathbf{v}_m-\mathbf{v}_k)+\nabla\cdot[\tau_k]+\dot{m}_k \mathbf{v}_k$$

5.3.3 Energy Equations

Gas Phase:

$$\frac{\partial}{\partial t}(\varepsilon_g \rho_g \mathbf{H}_g)+\nabla\cdot(\varepsilon_g \rho_g \mathbf{H}_g \mathbf{v}_g)=(\frac{\partial \mathbf{P}_g}{\partial t}+\mathbf{P}_g\nabla\cdot\mathbf{v}_g)+\nabla\cdot(\mathbf{k}_g\nabla\mathbf{T}_g)+\Phi_g+\sum_i \mathbf{r}_{ig}\Delta\mathbf{H}_{ig}$$
$$+\sum_{m=\ell,s}\left\{\mathbf{h}_{vm}(\mathbf{T}_m-\mathbf{T}_g)+\beta_{gm}(\mathbf{v}_m-\mathbf{v}_g)^2-\dot{m}_m\mathbf{H}_g\right\}$$

Liquid and Solid Phase: ($k=\ell,s$)

$$\frac{\partial}{\partial t}(\varepsilon_k\rho_k H_k)+\nabla\cdot(\varepsilon_k\rho_k H_k v_k)=h_{vk}(T_g-T_k)+\sum_{m=g,\ell,s}\beta_{km}(v_m-v_k)^2+\dot{m}_k H_g$$
$$+\nabla\cdot(k_k\nabla T_k)+\sum_i r_{ik}\Delta H_{ik}+\Phi_k$$

5.3.4 Fluctuating Energy Equation: (k=ℓ,s)

$$\frac{3}{2}\left[\frac{\partial}{\partial t}(\varepsilon_k\rho_k\Theta_k)+\nabla\cdot(\varepsilon_k\rho_k\Theta_k v_k)\right]=\nabla\cdot(\kappa_k\nabla\Theta_k)-\gamma_k-3\beta_{kg}\Theta_k+\Phi_k$$

5.3.5 Constitutive Equations

$$\varepsilon_g+\varepsilon_\ell+\varepsilon_s=1$$

Equation of State:

$$\rho_g=\frac{\overline{M}_g P_g}{zRT_g}$$

Drag Coefficients: (k=ℓ,s) (Based on Ergun Equation)

$$\beta_{gk}=\beta_{kg}=150\frac{(1-\varepsilon_g)\varepsilon_k\mu_g}{(\varepsilon_g d_k\psi_k)^2}+1.75\frac{\rho_g\varepsilon_k|v_g-v_k|}{\varepsilon_g d_k\psi_k} \qquad \varepsilon_g>0.8$$

$$\beta_{gk}=\beta_{kg}=\frac{3}{4}C_D\frac{\rho_g\varepsilon_k|v_g-v_k|}{d_k\psi_k}\varepsilon_g^{-2.65} \qquad \varepsilon_g<0.8$$

$$\beta_{\ell s}=\beta_{s\ell}=\frac{3}{2}(1+e)\frac{\rho_s\rho_\ell\varepsilon_s\varepsilon_s|v_\ell-v_s|}{\rho_s d_s^3+\rho_\ell d_\ell^3}(d_s+d_\ell)^2$$

where

$$C_D=\frac{24}{Re_k}(1+0.15Re_k^{0.687})$$

$$Re_k=\frac{\rho_g\varepsilon_g|v_g-v_k|d_k\psi_k}{\mu_g} \qquad Re_k=1000 \quad \text{if} \quad Re_k>1000$$

External Forces Acting on Each Phase

$$F_g = \frac{g}{\varepsilon_g}$$

$$F_k = \frac{g}{\varepsilon_g}\left(1 - \frac{1}{\rho_k}\sum_{m=g,\ell,s}\varepsilon_m \rho_m\right) \qquad k=\ell,s$$

Enthalpy:

$$H_g = C_{p_g}(T_g - T_g^0)$$

$$H_k = C_{p_k}(T_k - T_k^0)$$

Gas-Solid Heat Transfer: (Gunn's Model)

$$Nu_k = \left\{(2+5\varepsilon_k^2)(1+0.7Re_k^{0.2}Pr^{1/3}) + \left(\frac{2}{15}+1.2\varepsilon_k^2\right)Re_k^{0.7}Pr^{1/3}\right\}Sp_k$$

$$Nu_k = \frac{h_{vk}d_k}{k_g^0} \qquad Pr = \frac{C_{p_g}\mu_g}{k_g^0} \qquad Sp_k = \frac{6\varepsilon_k}{d_k}$$

Gas Phase Heat Transfer:

$$k_g^0 = 8.65\times10^5\left(\frac{T_g}{1400}\right)^{1.786}$$

$$k_g = (1-\sqrt{1-\varepsilon_g})k_g^0$$

Particulate Phase Heat Transfer:

$$\frac{k_k}{k_g^0} = \frac{\sqrt{\varepsilon_s}}{(1-\varepsilon_g)}\left\{\varphi\frac{k_k^*}{k_g^0} + (1-\varphi)\frac{k_k^0}{k_g^0}\right\}$$

$$\frac{k_k^0}{k_g^0} = \frac{2}{A_k}\left\{\frac{B_k\left\{(k_k^*/k_g^0)-1\right\}}{A_k^2(k_k^*/k_g^0)}\ln\frac{(k_k^*/k_g^0)}{B_k} - \frac{B_k-1}{A_k} - \frac{B_k+1}{2}\right\}$$

where

$$A_k = 1 - \frac{B_k}{(k_k^*/k_g^0)}$$

$$B_k = 1.25\left(\frac{\varepsilon_k}{\varepsilon_g}\right)^{10/9}(1+3\chi)$$

$$\chi = \sqrt{\frac{\left(\sum \varepsilon_k \rho_k\right)\left(\sum \varepsilon_k \rho_k / d_k^2\right)}{\left(\sum \varepsilon_k \rho_k / d_k\right)^2} - 1} \qquad k = l,s$$

$$k_k^* = 0.3289 \qquad \varphi = 7.26\times 10^{-3}$$

Shear Stresses:

$$[\tau_g] = \left\{-P_g - \frac{2}{3}\mu_g \varepsilon_g \nabla \cdot v_g\right\}[I] + \mu_g \varepsilon_g \left[\nabla v_g + (\nabla v_g)^T\right]$$

$$[\tau_k] = \left\{-P_k + \tau_{ck} + \left(\xi_k - \frac{2}{3}\mu_k\right)\nabla \cdot v_k\right\}[I] + \mu_k \left[\nabla v_k + (\nabla v_k)^T\right] \qquad k = \ell,s$$

Cohesive Force:

$$\tau_{ck} = 10^{10.6\varepsilon_k + 5.5} \qquad k = \ell,s$$

Solids Pressure and Viscosity Defined by Granular Temperature: ($k = \ell,s$)

$$P_k = \rho_k \varepsilon_k \Theta_k \{1 + 2(1+e_k) g_{0k} \varepsilon_k\}$$

$$\xi_k = \frac{4}{3}\varepsilon_k^2 \rho_k d_k g_{0k}(1+e_k)\sqrt{\frac{\Theta_k}{\pi}}$$

$$\mu_k = \frac{2\mu_{k_{dl}}}{(1+e_k)g_{0k}}\left\{1 + \frac{4}{5}(1+e_k)g_{0k}\varepsilon_s\right\}^2 + \frac{4}{5}\varepsilon_k^2 \rho_k d_k g_{0k}(1+e_k)\sqrt{\frac{\Theta_k}{\pi}}$$

$$\gamma_k = 3(1-e_k^2)\varepsilon_k^2 \rho_k g_{0k} \Theta_k \left\{\frac{4\sqrt{\Theta_k}}{d_k\sqrt{\pi}} - \nabla \cdot v_k\right\}$$

$$\kappa_k = \frac{2\kappa_{k_{dl}}}{(1+e_k)g_{0k}}\left\{1 + \frac{6}{5}(1+e_k)g_{0k}\varepsilon_k\right\}^2 + 2\varepsilon_k^2 \rho_k d_k g_{0k}(1+e_k)\sqrt{\frac{\Theta_k}{\pi}}$$

Where

$$g_{0k}=\left\{1-\left(\frac{\varepsilon_k}{\varepsilon_{k_{max}}}\right)^{1/3}\right\}^{-1} \qquad \mu_{k_{col}}=\frac{5}{96}\rho_k d_k\sqrt{\pi\Theta_k} \qquad \kappa_{k_{col}}=\frac{75}{384}\rho_k d_k\sqrt{\pi\Theta_k}$$

Energy Production Rate:

$$\Phi_k=[\tau_k]:\nabla v_k \qquad k=g,\ell,s$$

5.4 Operating Conditions

The operating conditions are same as those of LaPorte's RUN E-8.1 (Air Products 1991). Figure 5.1 shows reactor grid employed in this simulation. Gas passes through and slurry stays in the reactor.

Diameter of the reactor	57cm
Height of the reactor	813cm
Superficial gas velocity	15.24 cm/s
Superficial liquid velocity	0 cm/s
Superficial solid velocity	0 cm/s
Temperature	250.3 ^{o}C
Pressure	753.2 psig
Catalyst diameter	50 μm
Liquid	wax
Density of liquid	0.70025 g/cm^3
Grid size (dx & dy)	1.68cm x 20.3 cm
Number of cells in the grid	34x40
Time interval	10^{-4} sec.

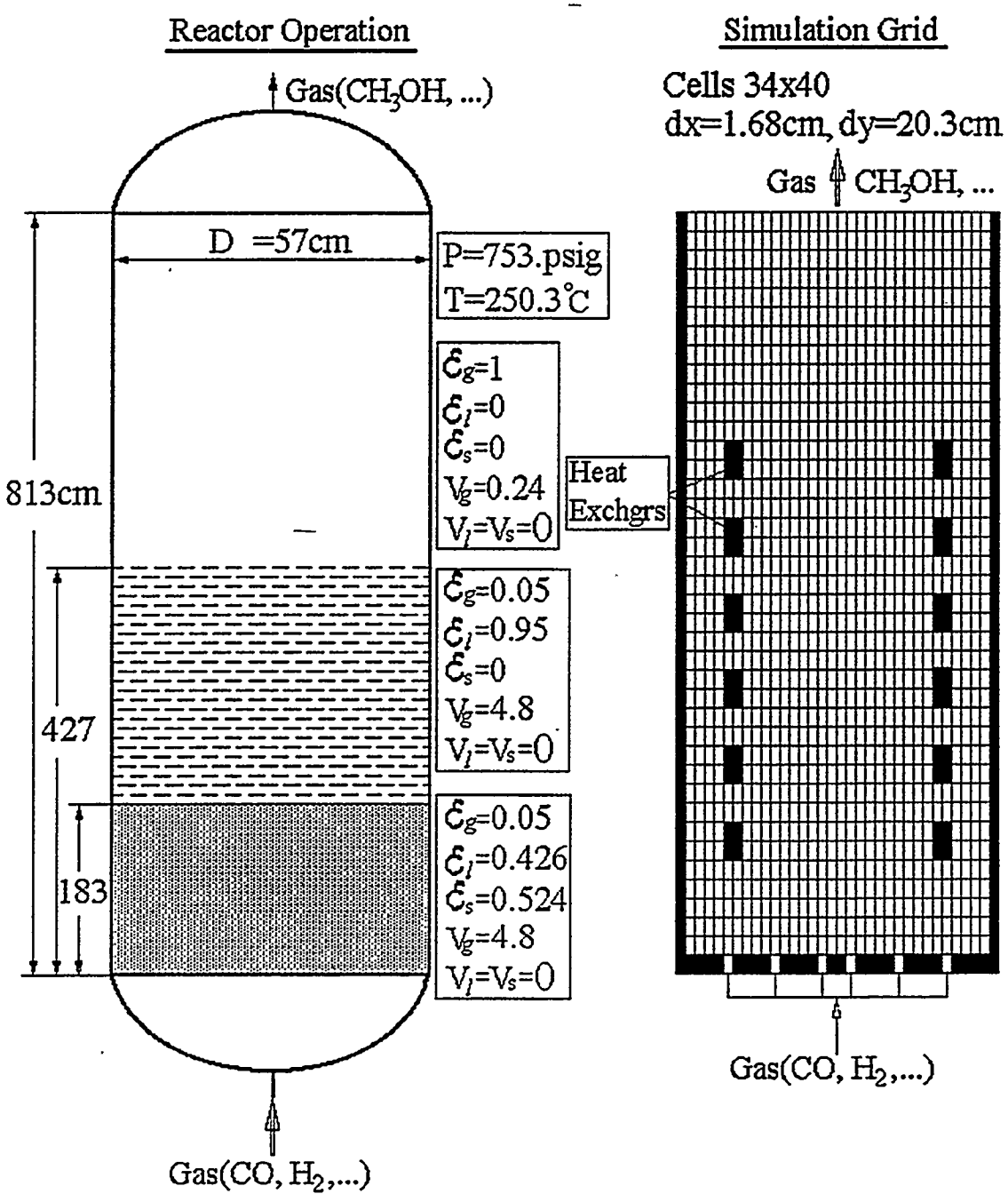

Figure 5.1 Reactor Operation without Slurry Circulation and Simulation Grid

5.5 Numerical Considerations

5.5.1 Initial Conditions. A constant pressure, 753.2 psig, is kept at the top of the reactor. The initial conditions are summerized as followings:

	gas	liquid	solid
0 – 183	$\varepsilon_g = 0.050$	$\varepsilon_\ell = 0.426$	$\varepsilon_s = 0.524$
	$v_g = 4.8$	$v_\ell = 0$	$v_s = 0$
	$u_g = 0$	$u_\ell = 0$	$u_s = 0$
183 – 427	$\varepsilon_g = 0.050$	$\varepsilon_\ell = 0.950$	$\varepsilon_s = 0.000$
	$v_g = 4.8$	$v_\ell = 0$	$v_s = 0$
	$u_g = 0$	$u_\ell = 0$	$u_s = 0$
427 – 813	$\varepsilon_g = 1.000$	$\varepsilon_\ell = 0.000$	$\varepsilon_s = 0.000$
	$v_g = 0.24$	$v_\ell = 0$	$v_s = 0$
	$u_g = 0$	$u_\ell = 0$	$u_s = 0$

Syn-gas composition (CO-rich):

		CO	CO_2	H_2	N_2	CH_3OH
%mol		51	13	35	1	0
y_g^j	%wt	68.07	27.26	3.34	1.33	0

5.5.2 Boundary Conditions. The thermal boundary conditions around the computing mesh and a heat block are summerized as following.

Boundaries:

$$\frac{\partial T_k}{\partial r}=0 \qquad \frac{\partial T_k}{\partial y}=0 \qquad k=g,\ell,k$$

Around heat block:

Case 1. constant heat flux

$$\frac{\partial T_k}{\partial x}=C_{fx}\cdot\varepsilon_k \qquad \frac{\partial T_k}{\partial y}=C_{fy}\cdot\varepsilon_k \qquad k=g,\ell,k$$

Case 2. constant block temperature T_B

$$\frac{\partial T_k}{\partial x}=K_x\cdot\varepsilon_k(T_B-T_k) \qquad \frac{\partial T_k}{\partial y}=K_y\cdot\varepsilon_k(T_B-T_k) \qquad k=g,\ell,k$$

The inflow conditions, including gas velocity and composition, and the top pressure are prescribed. Assumption of non-slip at the walls is made for both gas and liquid phases. The boundary conditions around the computing mesh, shown as Figure 5.1, are summerized as followings.

	gas	liquid	solid
bottom	$\varepsilon_g=1$	$\varepsilon_\ell=0$	$\varepsilon_s=0$
orifice	$v_g=81.3\text{cm/s}$	$v_\ell=0$	$v_s=0$
	$u_g=0$	$u_\ell=0$	$u_s=0$
	$y_g^j=y_g^{j0}$	$y_\ell^j=0$	$y_s^j=0$
left/right	$v_g=0$	$v_\ell=0$	$v_s=0$
	$u_g=0$	$u_\ell=0$	$u_s=0$
top	$\frac{\partial \varepsilon_g}{\partial y}=0$	$\frac{\partial \varepsilon_\ell}{\partial y}=0$	$\frac{\partial \varepsilon_s}{\partial y}=0$
	$\frac{\partial v_g}{\partial y}=0$	$\frac{\partial v_\ell}{\partial y}=0$	$\frac{\partial v_s}{\partial y}=0$
	$u_g=0$	$u_\ell=0$	$u_s=0$
	$\frac{\partial y_g^j}{\partial y}=0$	$\frac{\partial y_\ell^j}{\partial y}=0$	$\frac{\partial y_s^j}{\partial y}=0$

BLANK PAGE

5.5.3 Computation. Finite difference method is used to solve these partial differential equations simultaneously and the values of following variables at each time step and cell position can be obtained.

$$\varepsilon_g, \varepsilon_\ell, \varepsilon_s, v_g, v_\ell, v_s, P_g, y_g^j, y_\ell^j, y_s^j$$
$$j = CO, CO_2, H_2, N_2, CH_3OH, wax$$

5.6 Computational Results and Discussions

The initial state of the reactor is shown in Figure 5.1. The obstacles shown represent heat exchangers. At time zero, the syn-gas is injected to reactor through six orifices and the gas velocity is increased gradually to the final value during the first computing second. The total computing time is 80 seconds. The computing run was performed on a HP735 Workstation and the simulation time is 80 seconds. All values using in the follow figures and Tables are time and cross section area average over last 40 seconds.

Table 5.1 lists the material balance of the simulations and Table 5.2 lists the comparison of simulation and LaPorte's RUN E-8.1. They show very close CO conversion and rate of methanol production.

Figure 5.2 shows the time response of gas mass flowrate at reactor top. There are strong oscillations occurring during the first 4 seconds after start-up (syn-gas injection). After that, a hydrodynamic steady state could be assumed.

Figure 5.3 shows the time average gas-liquid-solid volume fraction profiles. Table 5.2 and Figure 5.3 also show that the height of slurry and gas holdup are roughly agree with RUN E-8.1.

Table 5.1 Material Balance: ($CO:H_2$=1.5:1)

	Inlet		Outlet	
	% mol	kgmol/hr	% mol	kgmol/hr
CO	51	87.9	51.18	74.8
CO_2	13	22.4	15.39	22.4
H_2	35	60.3	23.03	33.6
CH_3OH	0	0.0	9.20	13.4
N_2	1	1.7	1.18	1.7
$\overline{M}$ (kg/kgmol)	20.98		24.84	
Flowrate (kgmol/hr)		172.3		145.9
Flowrate (kg/hr)		3614		3625

Table 5.2 Comparison of Simulation and Air Products' (1991) RUN E-8.1:

	CO conv. (%)	gas holdup (%)	slurry height (inches)	total catalyst (kg)	CH_3OH (gmol/hr /kg)	net CH_3OH (TPD)
Simulation	14.24	26.9	215	740	16.93	9.62
RUN E-8.1	13.50	29.5	200	567	20.50	10.03

Figure 5.4 shows the comparison of methanol profile computed by (1993), one-dimensional steady state model and the two-dimensional hydrodynamic model. The one-dimensional model predicts a high methanol production because of the assumption of uniform catalyst concentration. The hydrodynamic model, however, predicts much close methanol production (Table 5.2) since it accounts the effect of the distribution of gas, catalyst concentrations, temperature and the flow patterns inside the reactor.

Figure 5.5a--d show the gas volume fraction distributions as a function of time. During the first 4 seconds after startup (syn-gas injection), irregular distributions reflect that the operation is non-stable which has been shown in Figure 5.2. After 4 seconds the

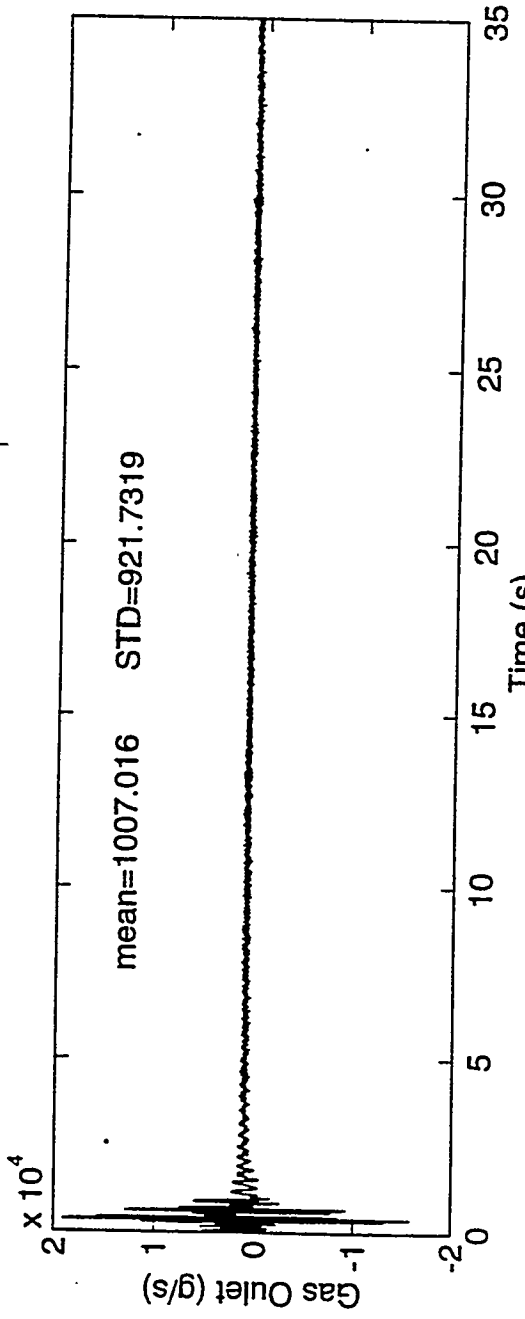

Figure 5.2 Gas Mass Flowrate at Reactor

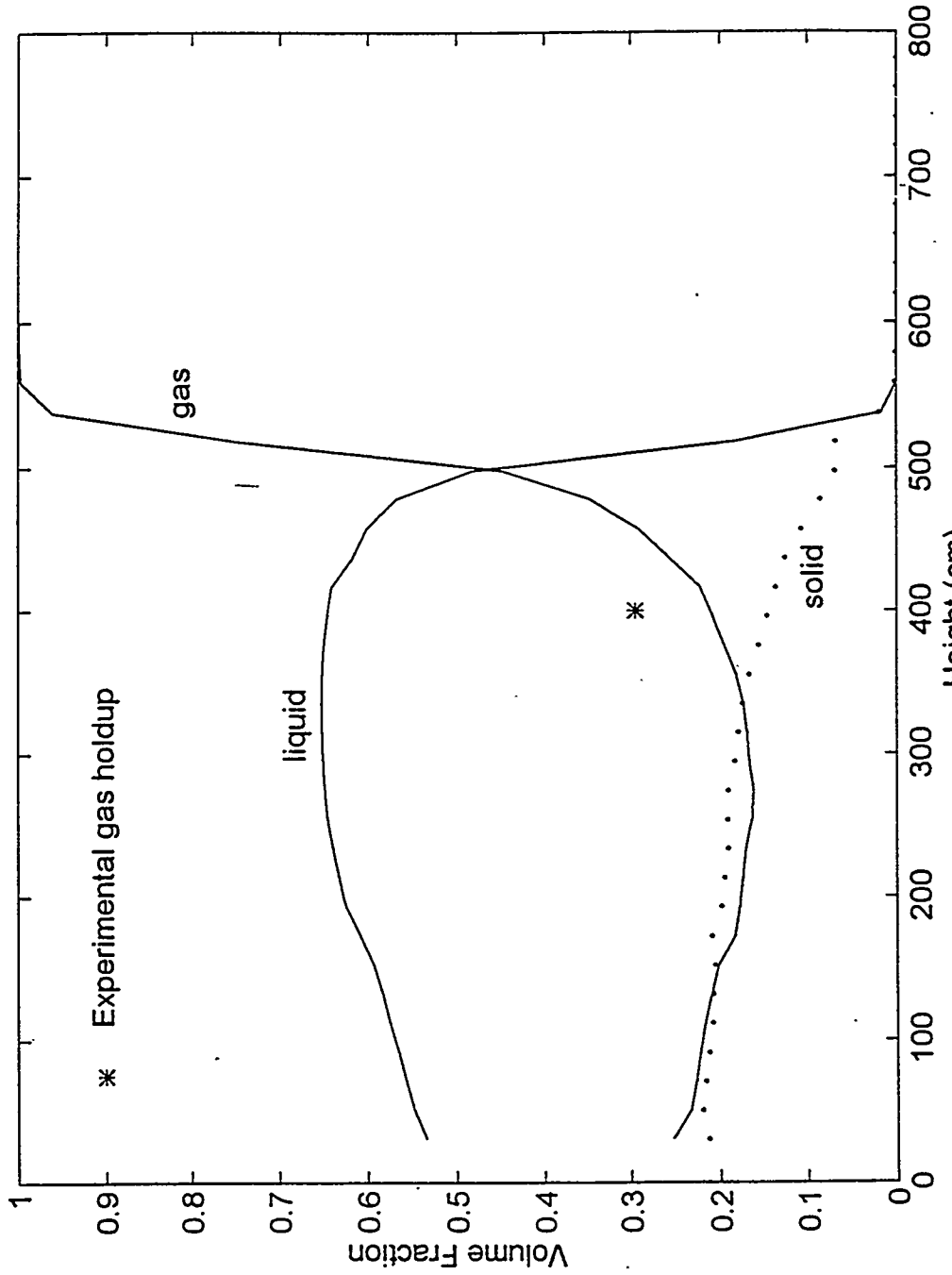

Figure 5.3 Time average G-L-S Volume Fraction

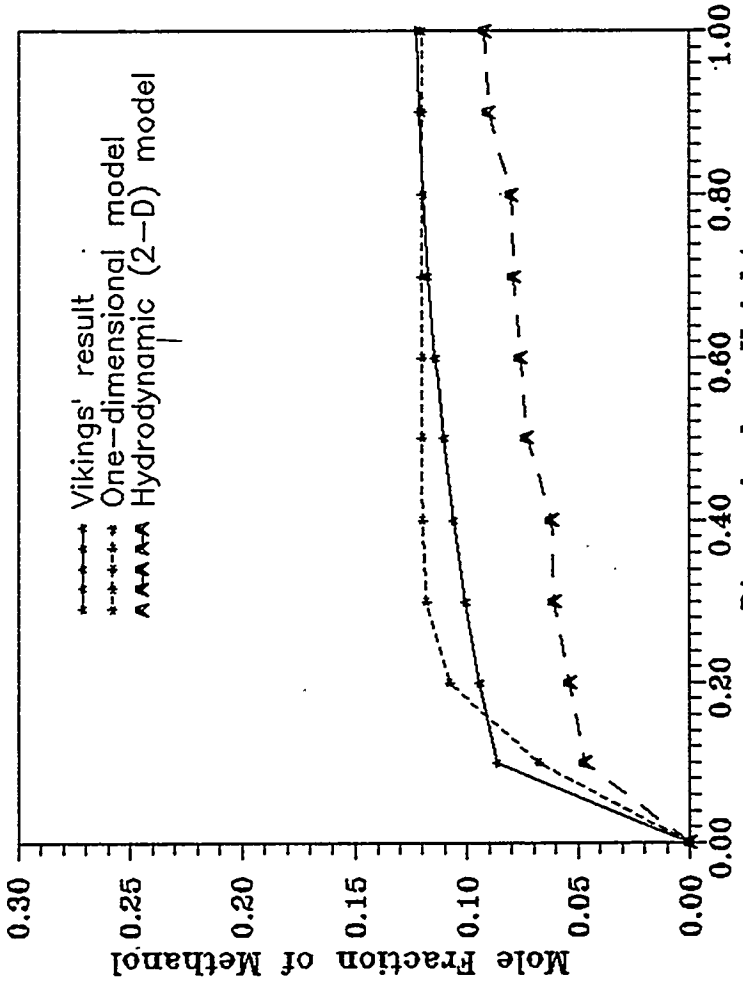

Figure 5.4 Methanol Concentration Profiles from IIT's Hydrodynamic, One-dimensional and Vikings' Models

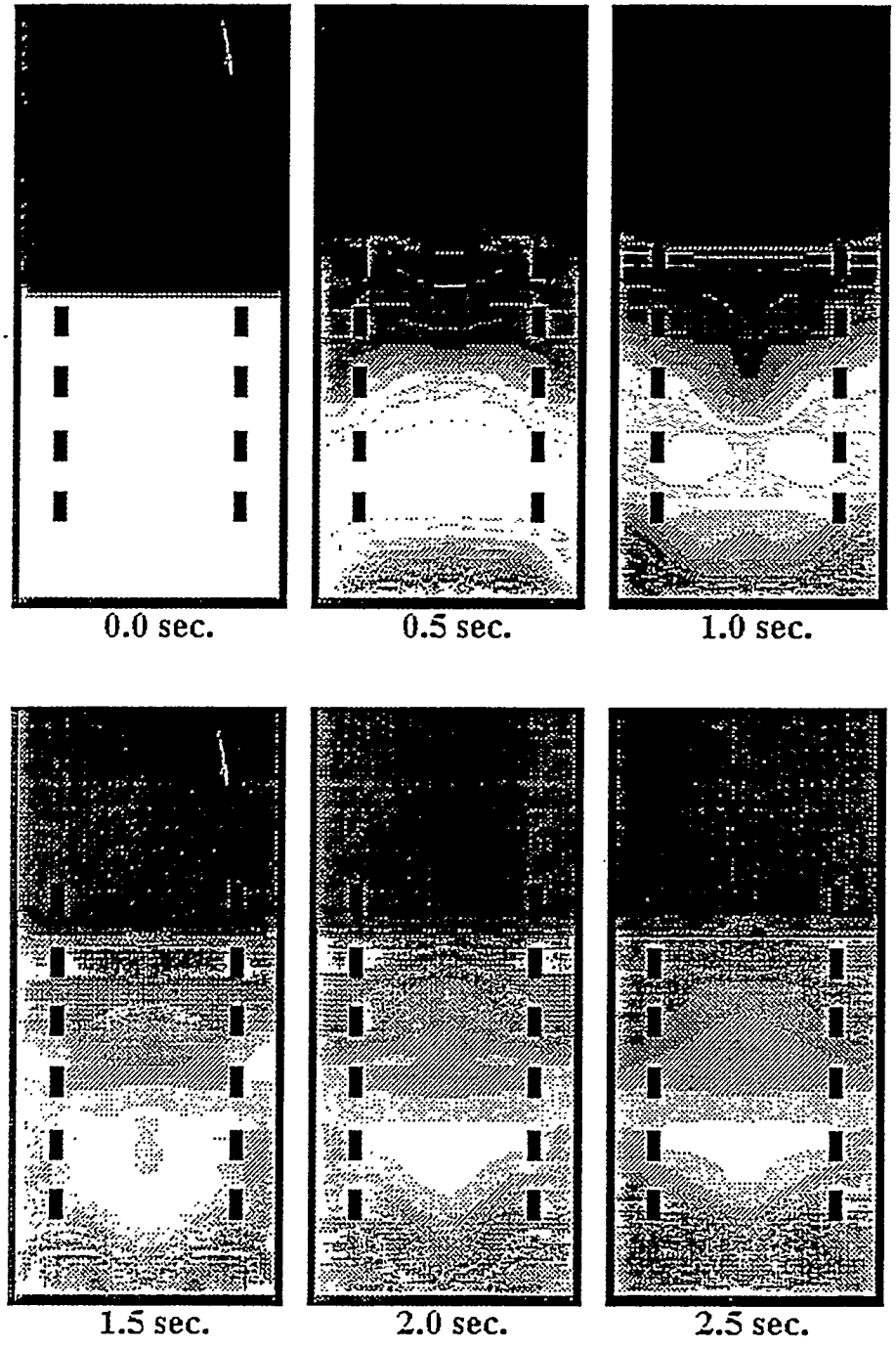

Figure 5.5a The Gas Volume Fraction Profiles as a Function of Time

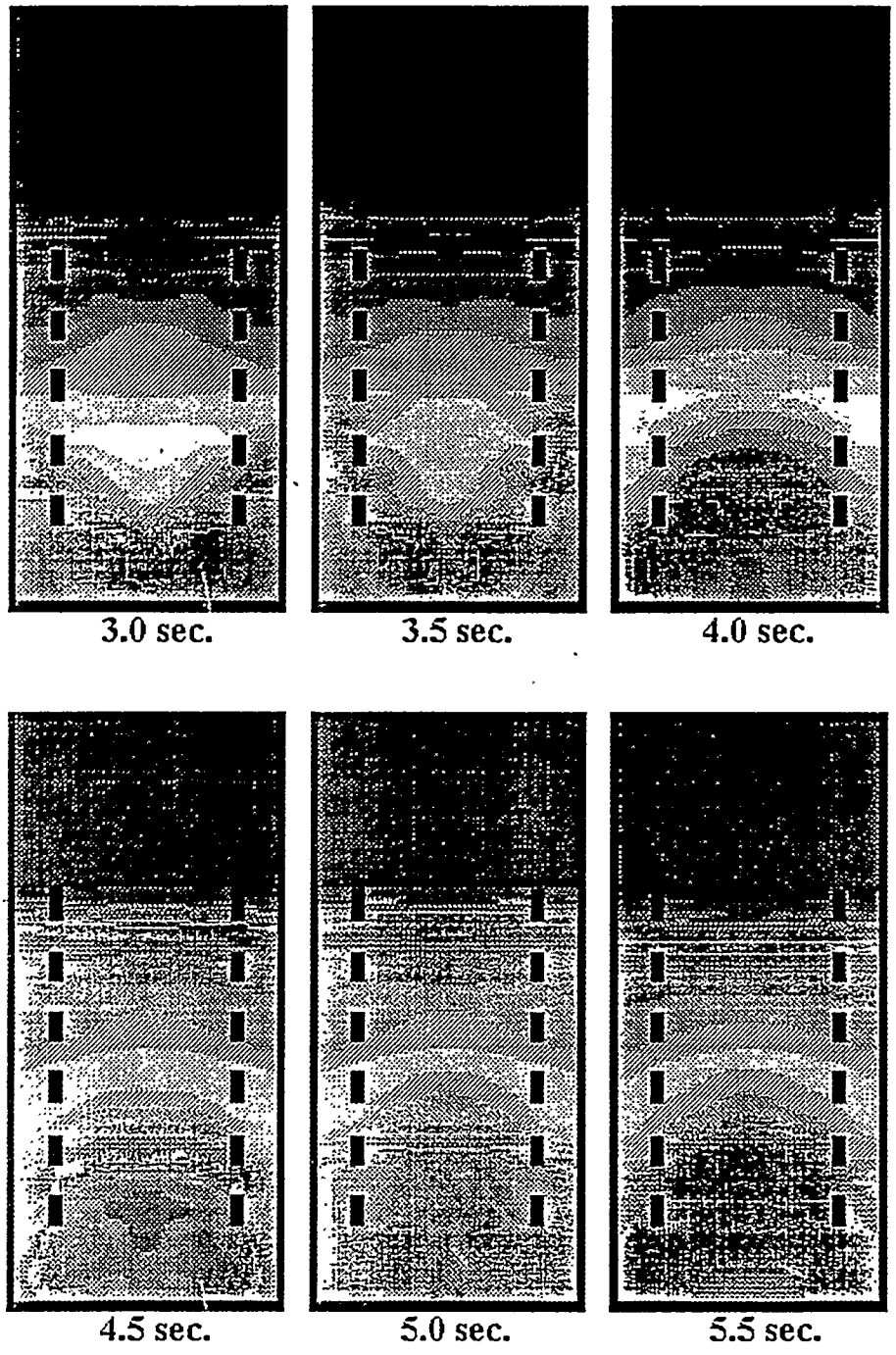

Figure 5.5b The Gas Volume Fraction Profiles as a Function of Time

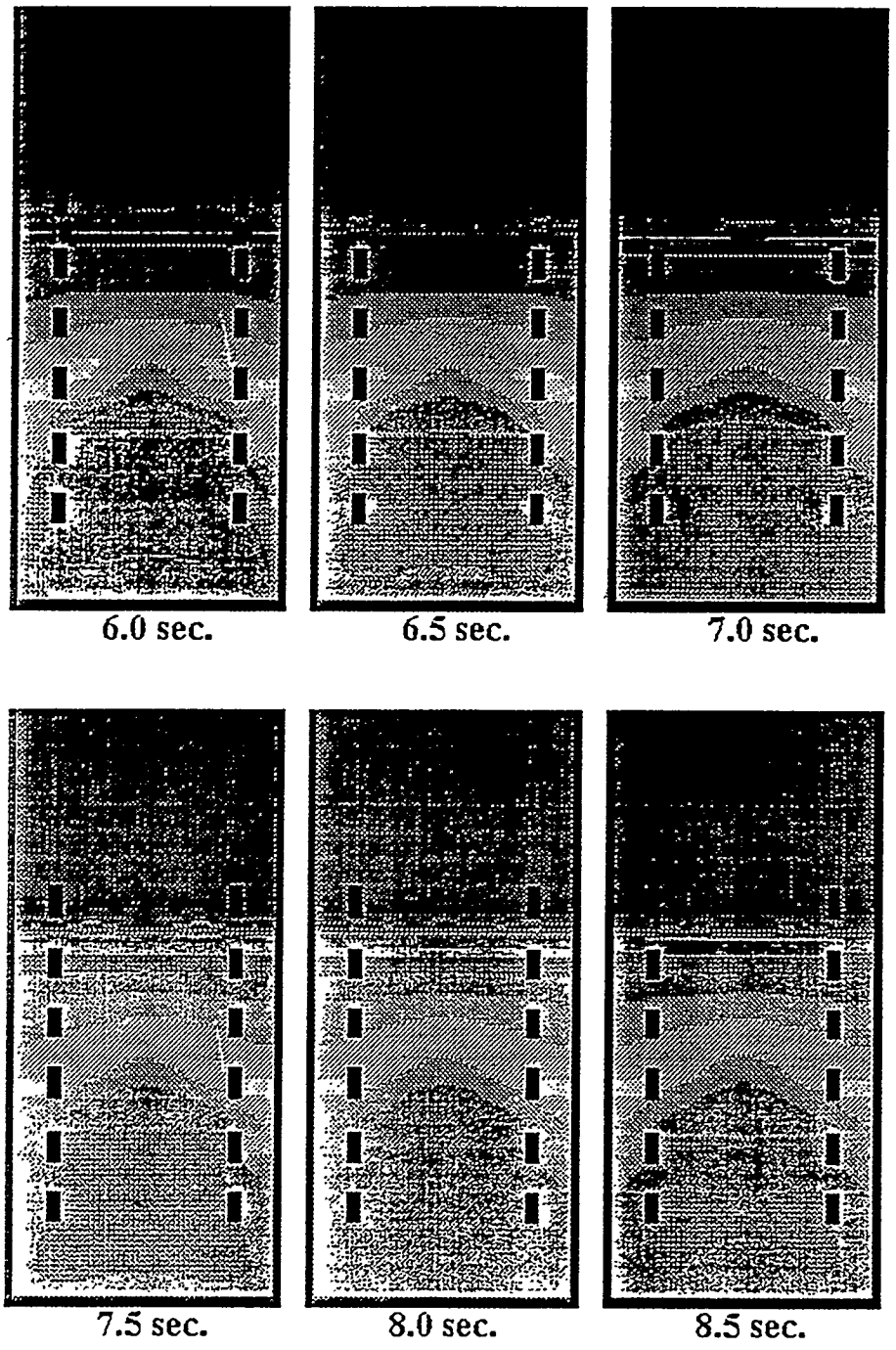

Figure 5.5c The Gas Volume Fraction Profiles as a Function of Time

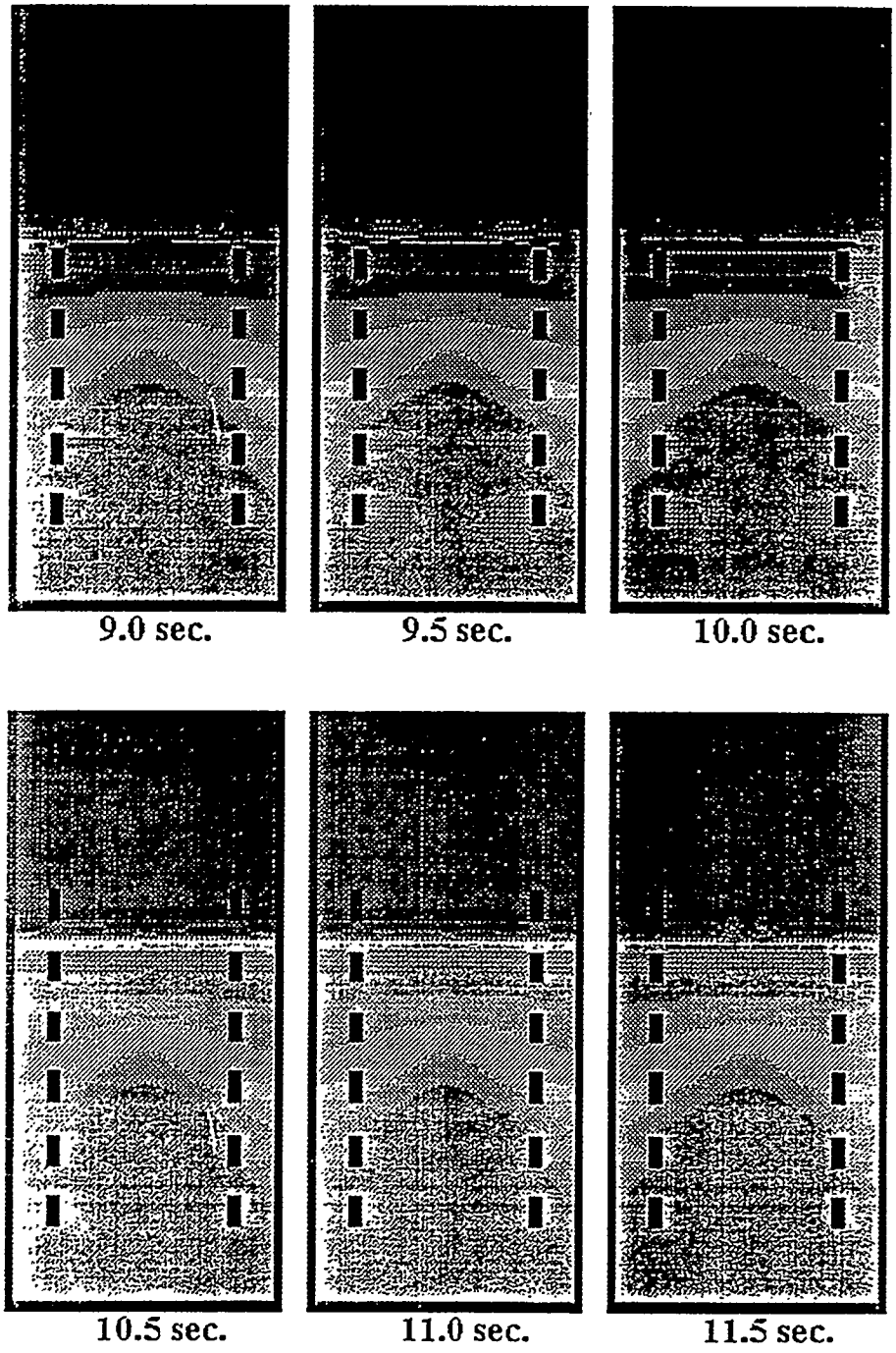

Figure 5.5d The Gas Volume Fraction Profiles as a Function of Time

operation approaches steady state in hydrodynamic sense. The gas volume fraction decreases along the elevation because of the reaction of methanol synthesis. These figures also demonstrate a non-uniform radial distribution that one-dimensional model could not predict.

Figure 5.6a--d show the catalyst volume fraction distributions varying with time. The catalyst expands rapidly after injection of syn-gas and settles down at steady state.

Figure 5.7a-e show the methanol concentration distributions varying with time. After injection of syn-gas to the methanol free reactor from six orifices, the methanol is forming, propagating rapidly and accumulating and its concentration reaches a steady value, 9% mole, which agrees with LaPorte's RUN E-8.1.

Figure 5.8a-c show the temperature distributions varying with time. The heat exchangers absorb heat released from the exothermal methanol synthesis reaction.

Figure 5.9 shows a transient distribution of the rate of methanol reaction.

Figure 5.10 and 5.11 show solid viscosity and granular temperature distributions. The viscosity and granular temperature are high at the reactor entrance due to the injection of syn-gas.

Figure 5.12 shows a transient gas flow pattern. There exists vortices inside the reactor and they imply the good mixing feature of slurry bubble column reactor.

Figure 5.13 shows a series of gas flow patterns as a function of time.

5.7 Convergence Check

The IIT's hydrodynamic code uses the finite difference method to solve the partial differential equations. The grid size is very sensitive to the stability and convergence of

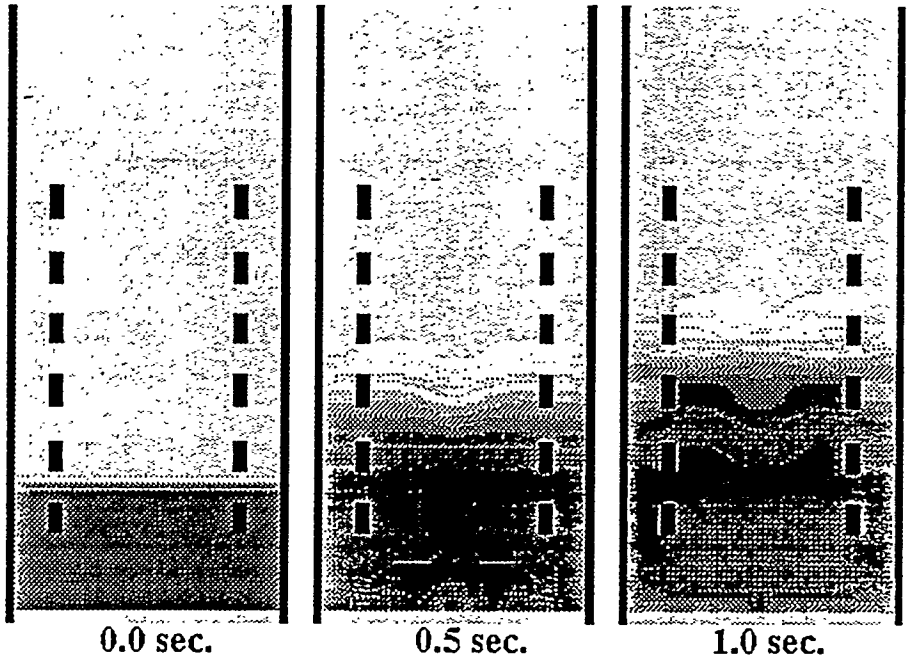

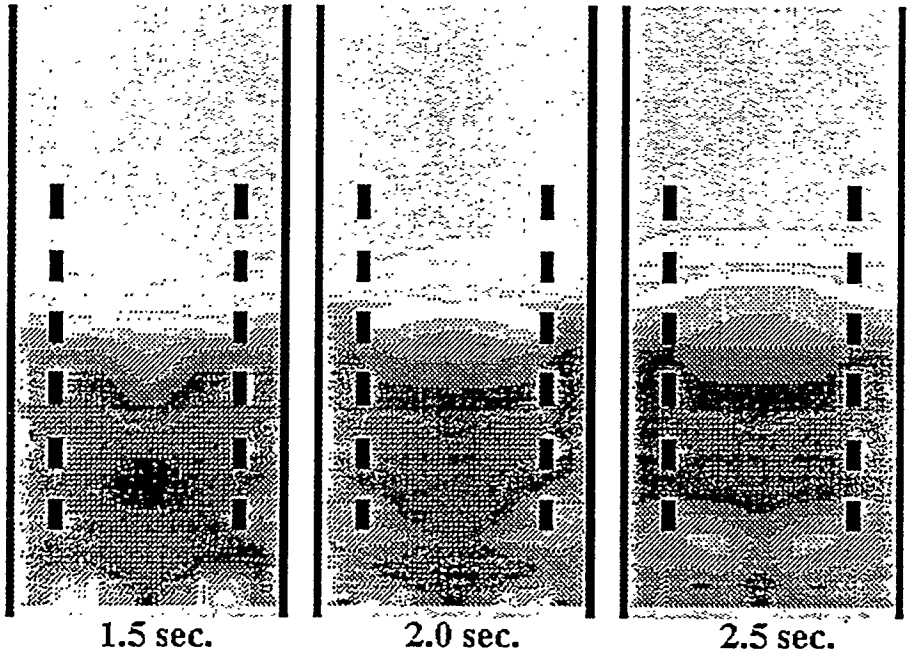

Figure 5.6a The Solid Volume Fraction Profiles as a Function of Time

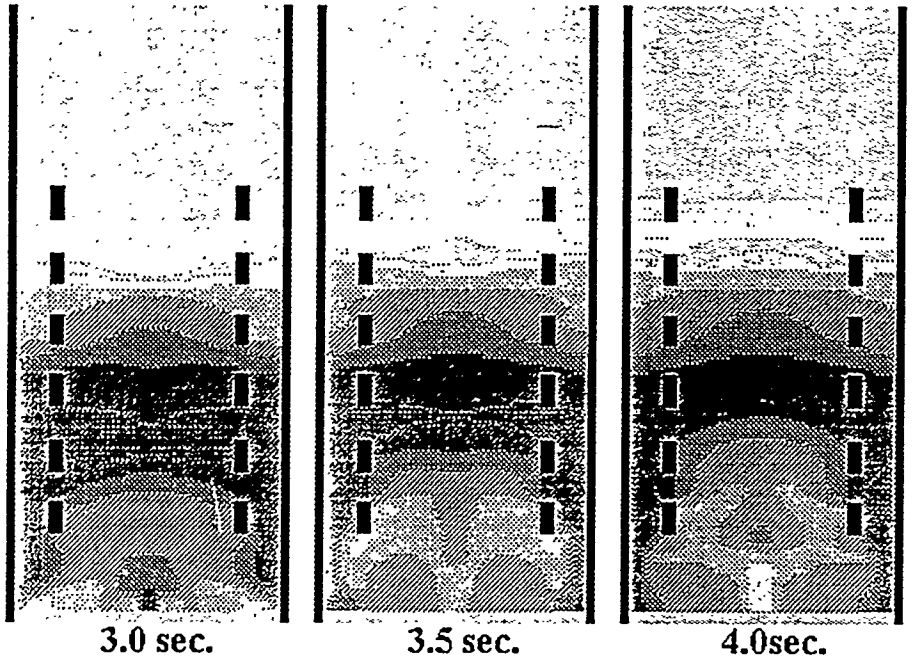

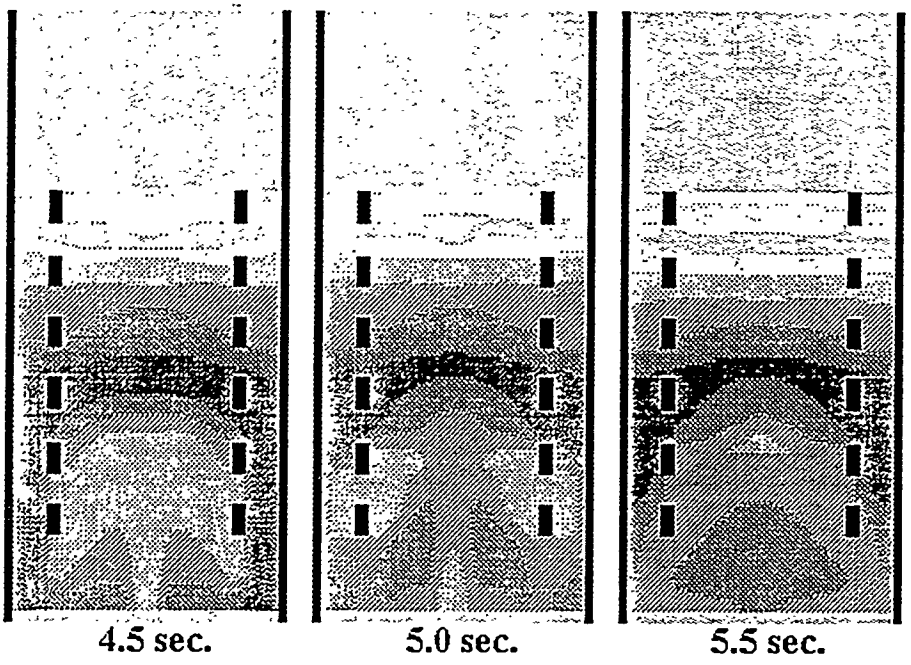

Figure 5.6b The Solid Volume Fraction Profiles as a Function of Time

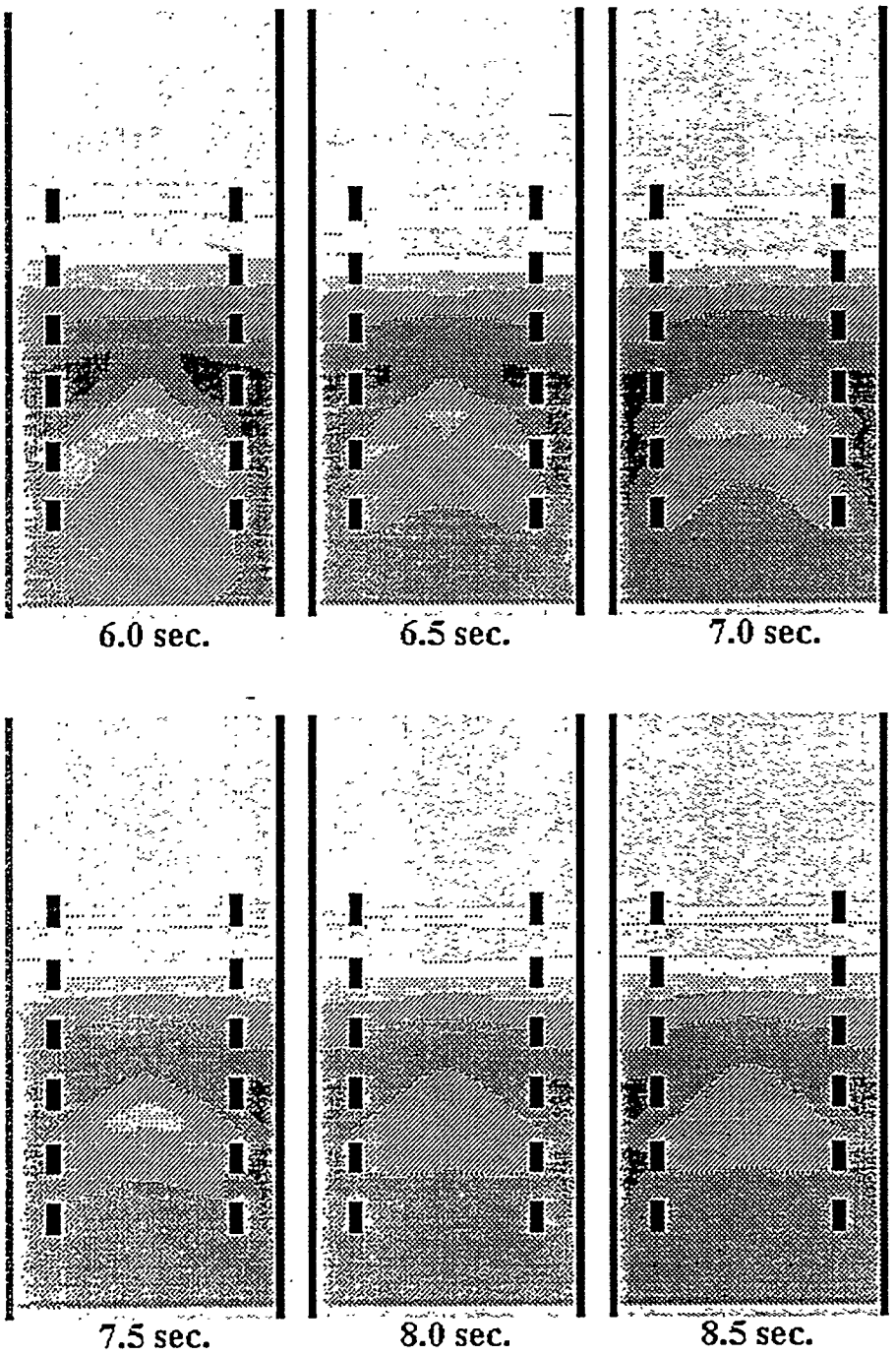

Figure 5.6c The Solid Volume Fraction Profiles as a Function of Time

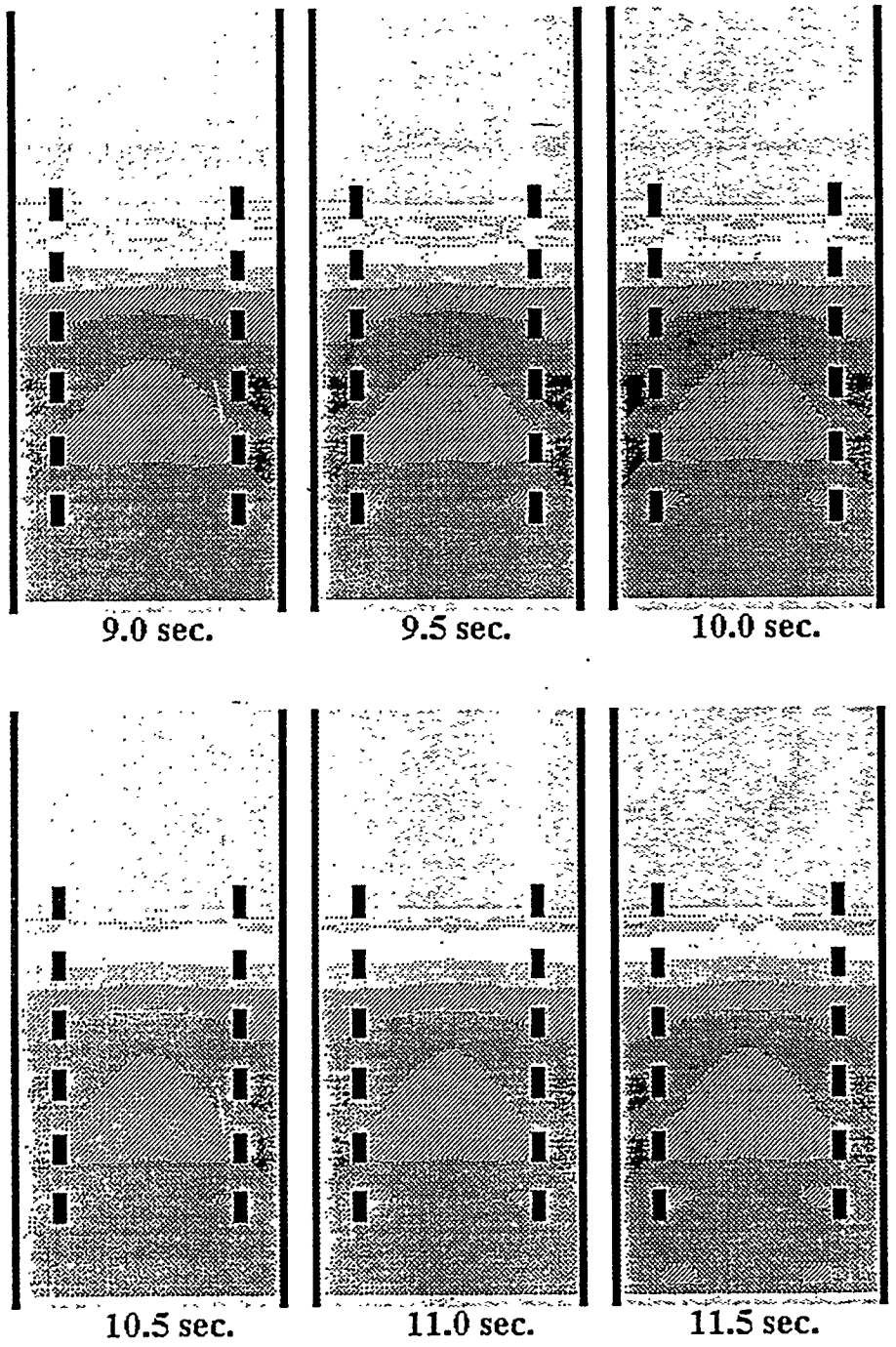

Figure 5.6d The Solid Volume Fraction Profiles as a Function of Time

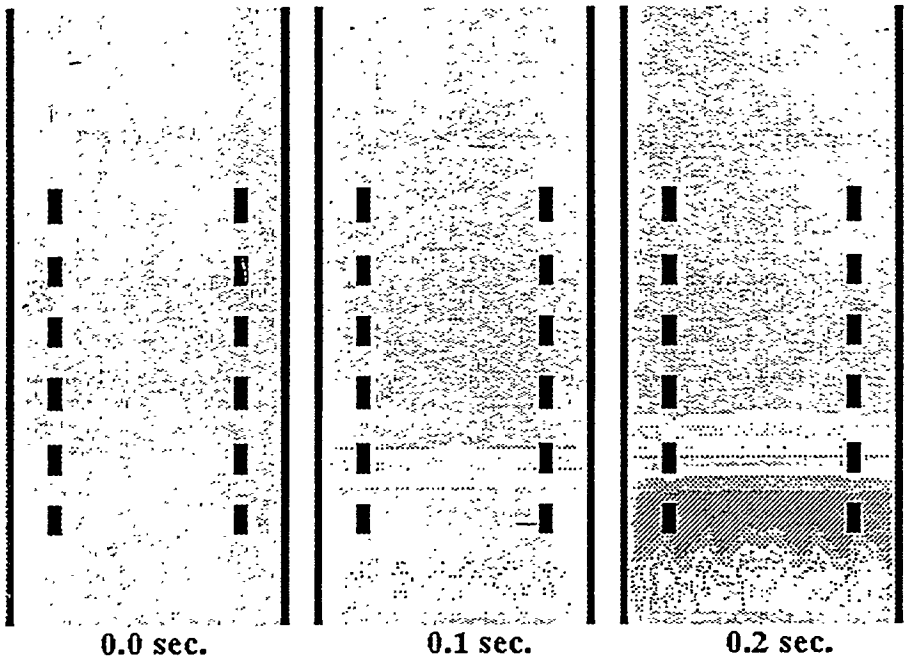

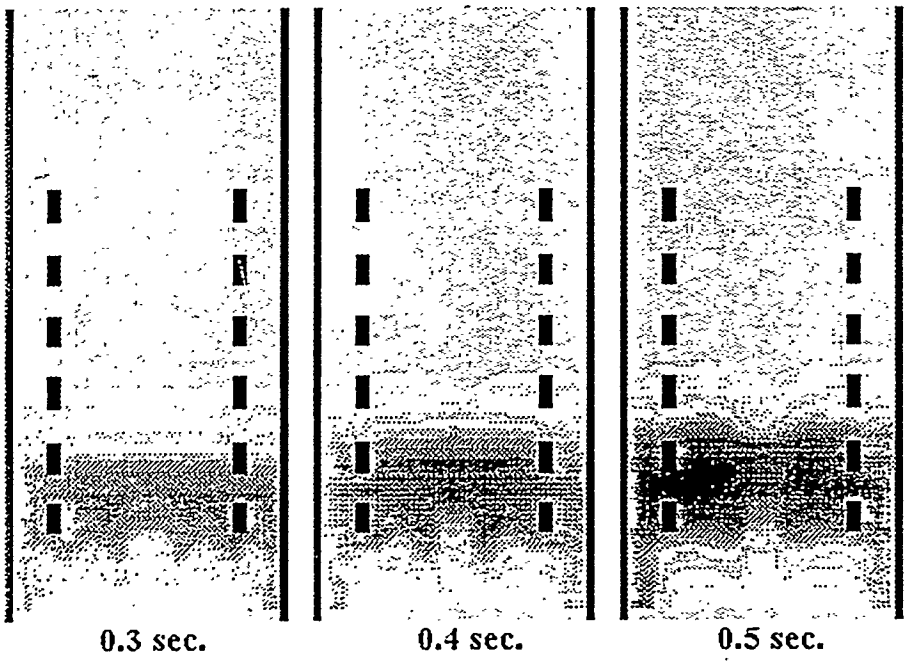

Figure 5.7a The Methanol Concentration Profiles as a Function of Time

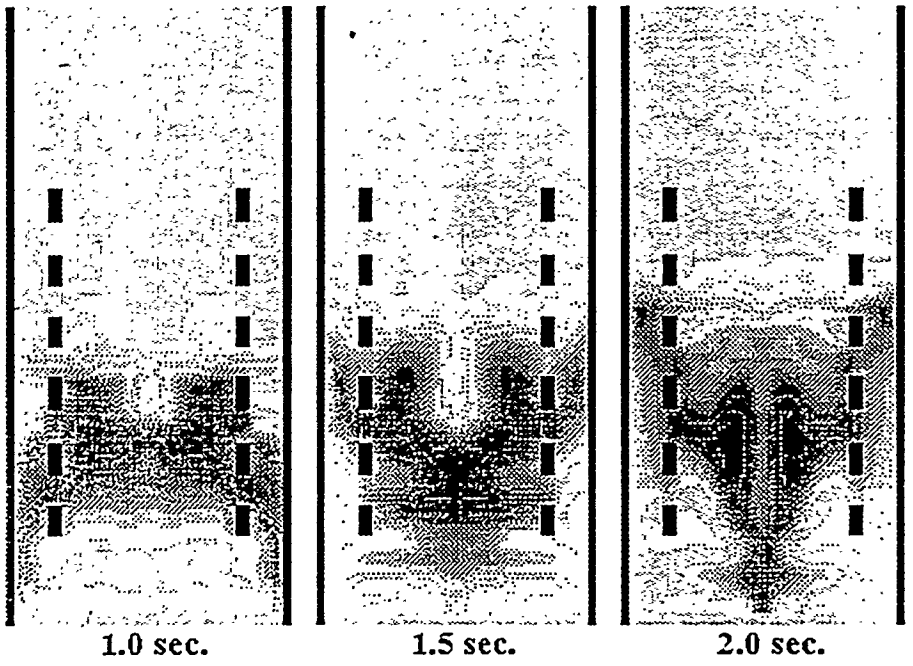

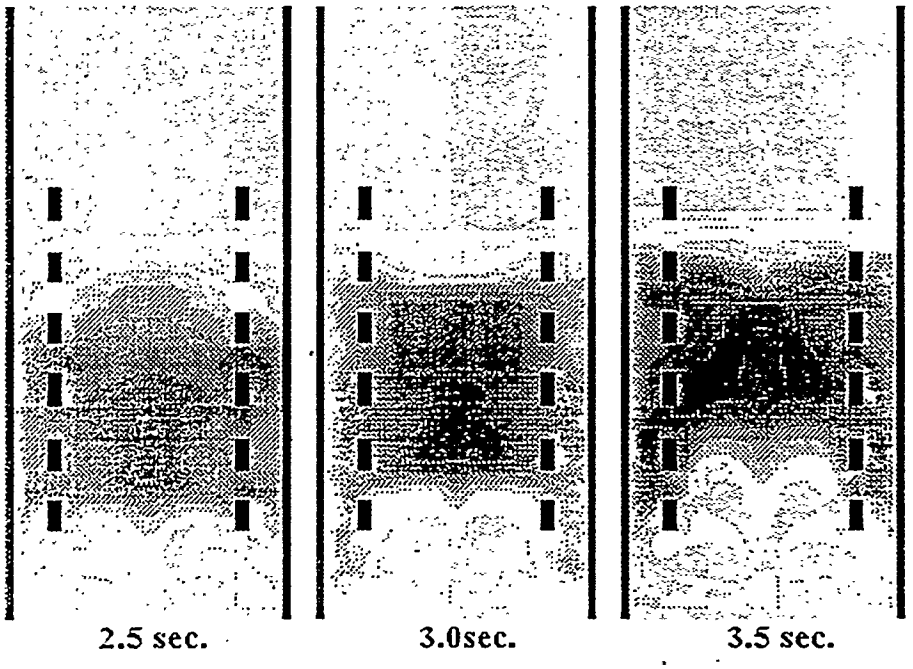

Figure 5.7b The Methanol Concentration Profiles as a Function of Time

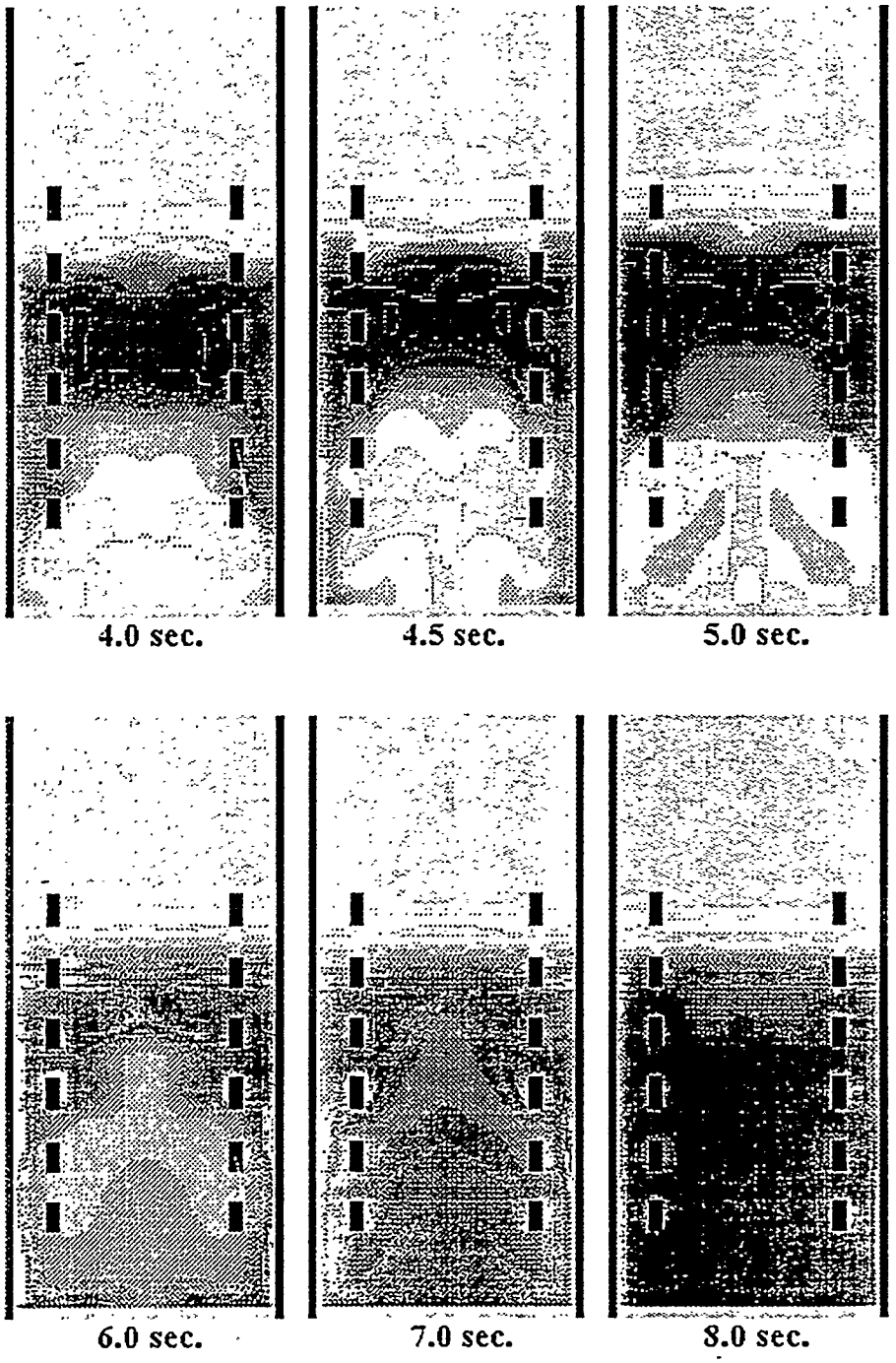

Figure 5.7c The Methanol Concentration Profiles as a Function of Time

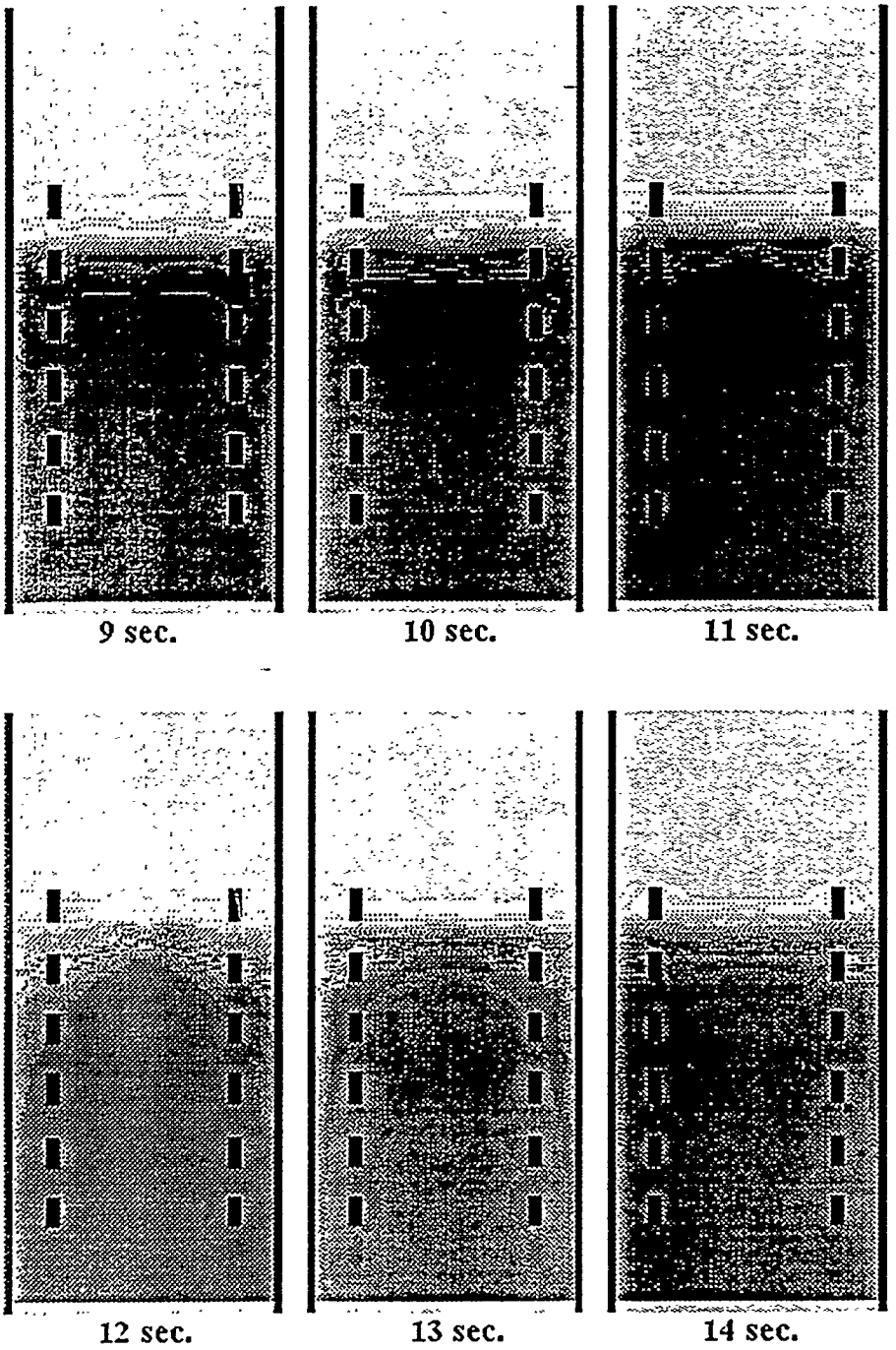

Figure 5.7d The Methanol Concentration Profiles as a Function of Time

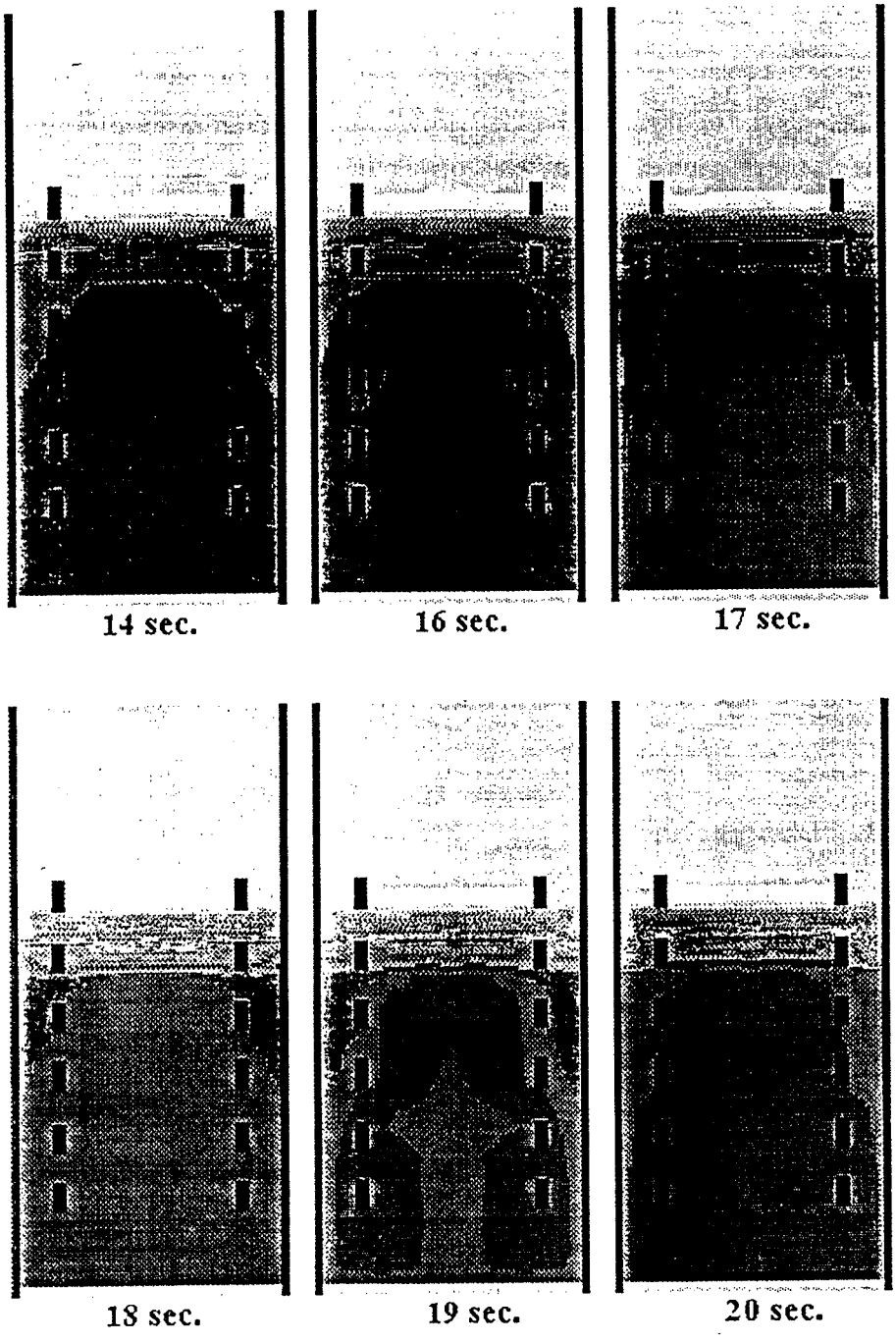

Figure 5.7e The Methanol Concentration Profiles as a Function of Time

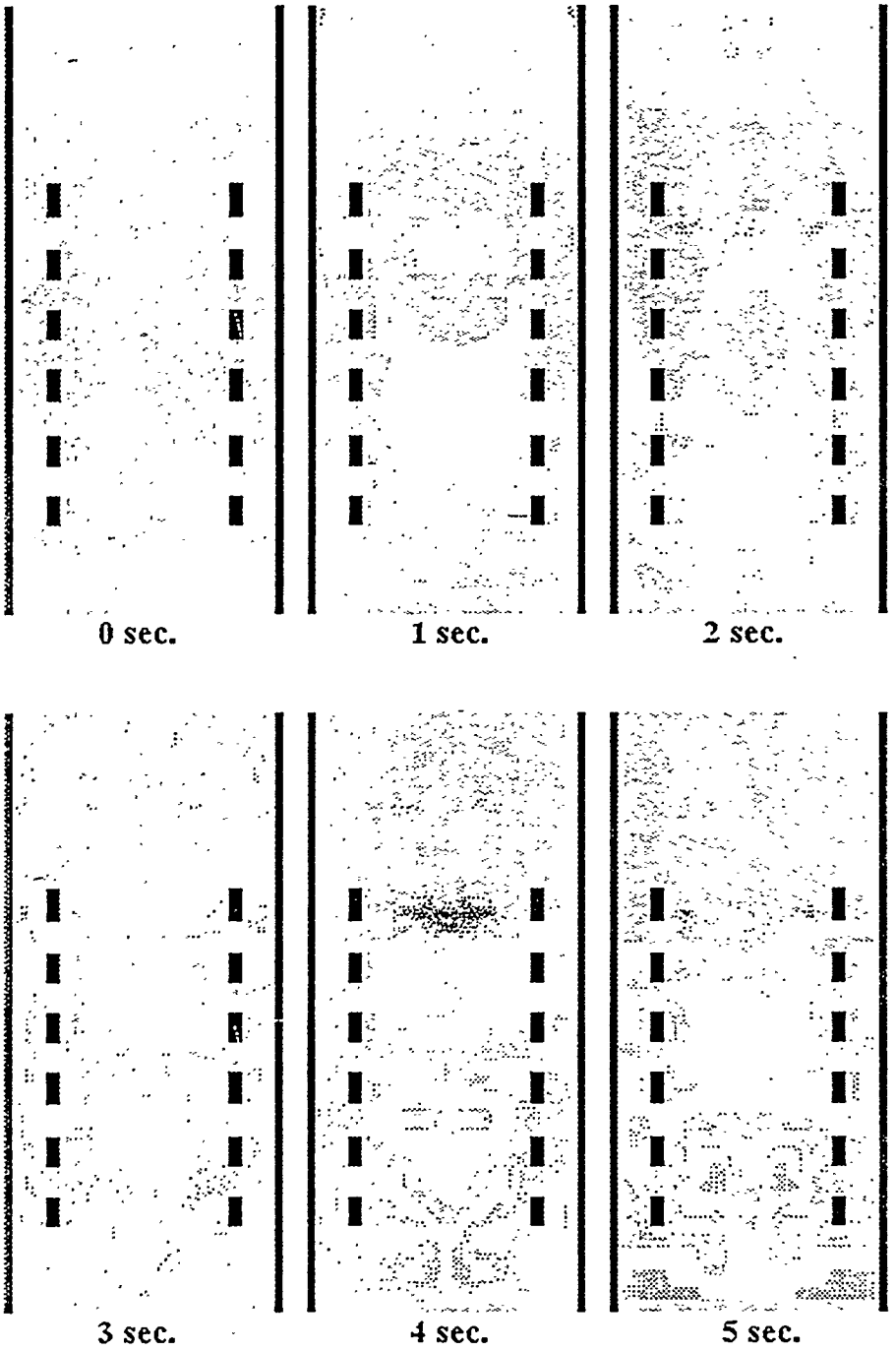

Figure 5.8a The Temperature Profiles as a Function of Time

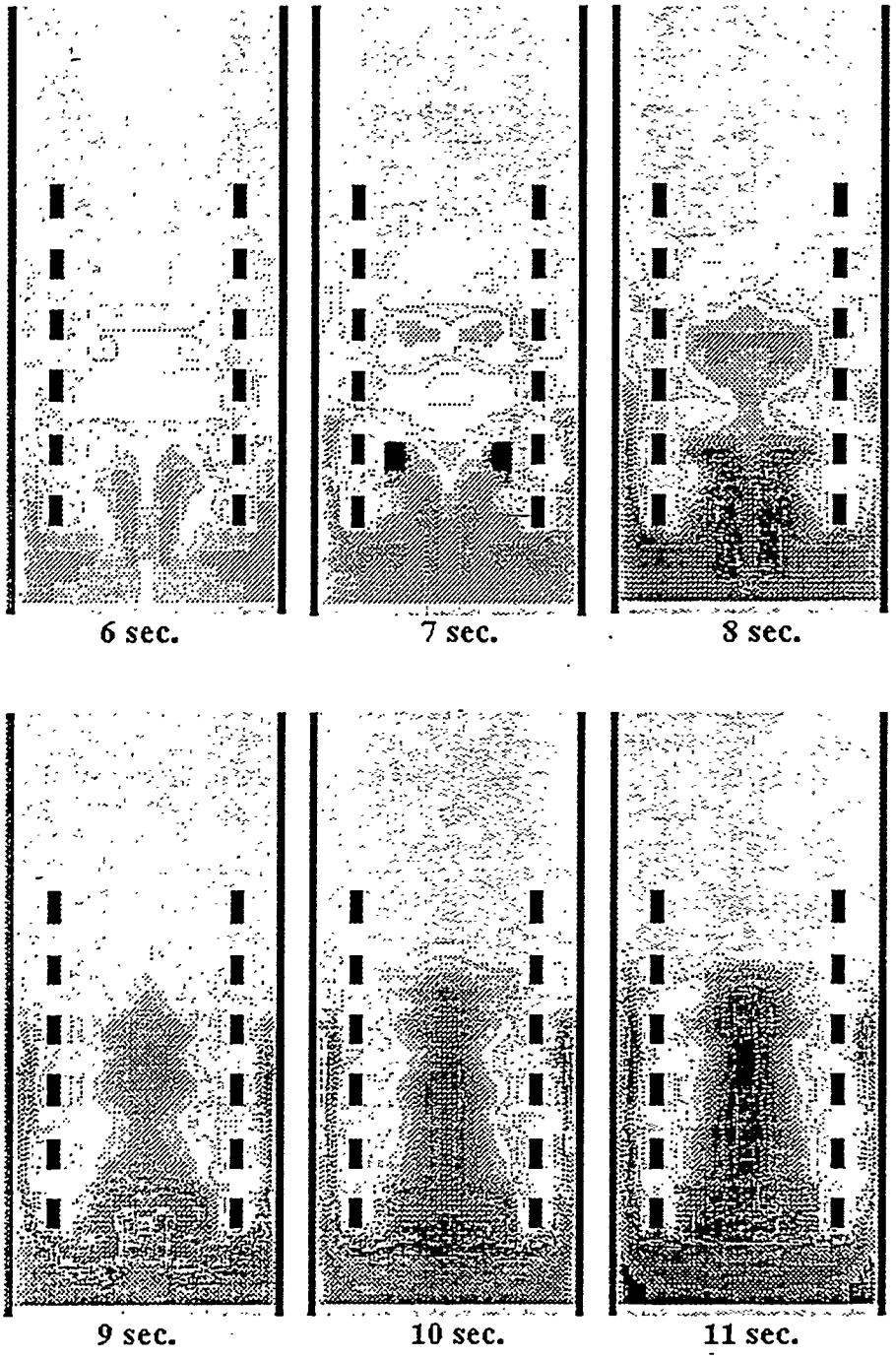

Figure 5.8b The Temperature Profiles as a Function of Time

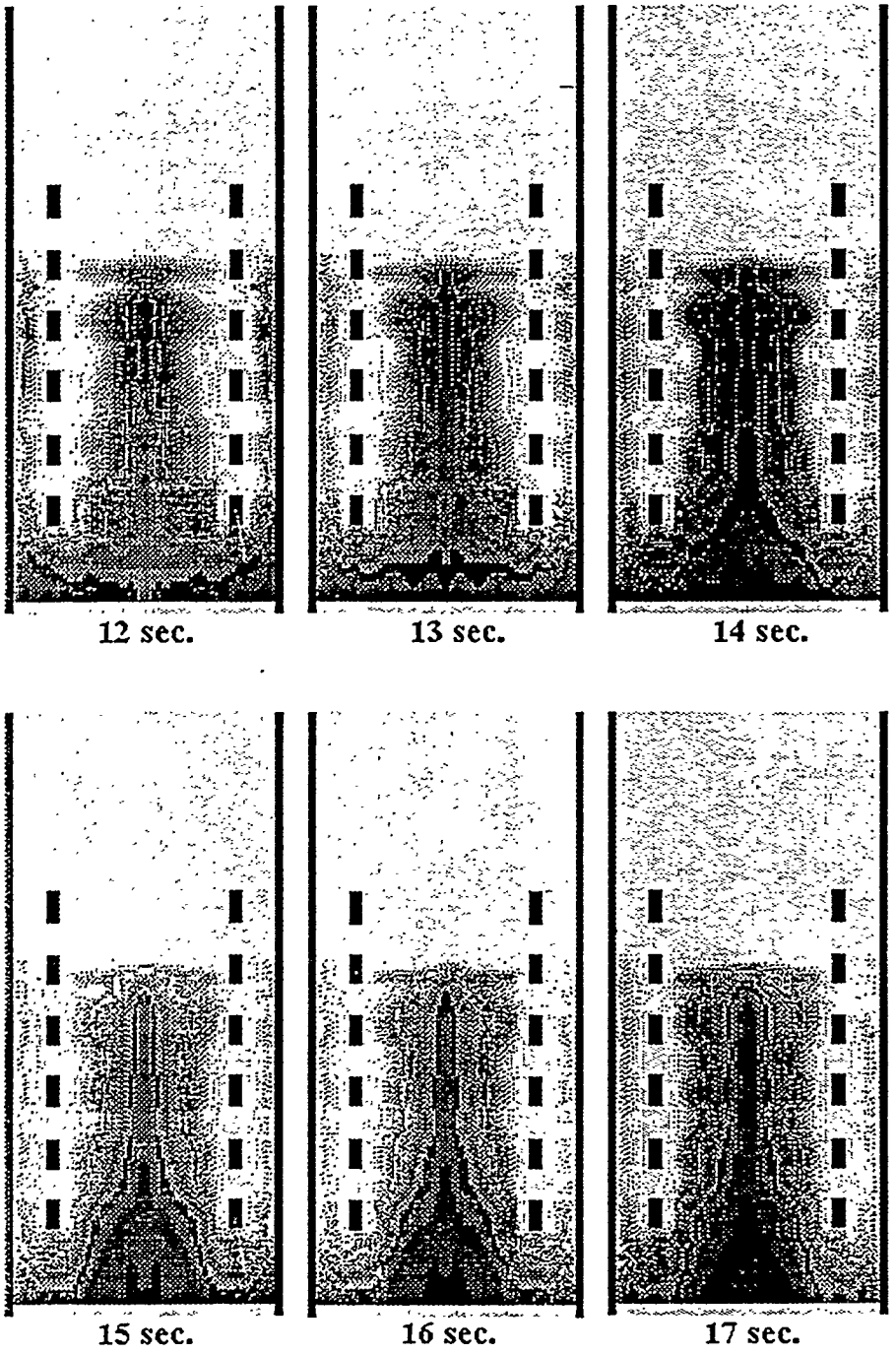

Figure 5.8c The Temperature Profiles as a Function of Time

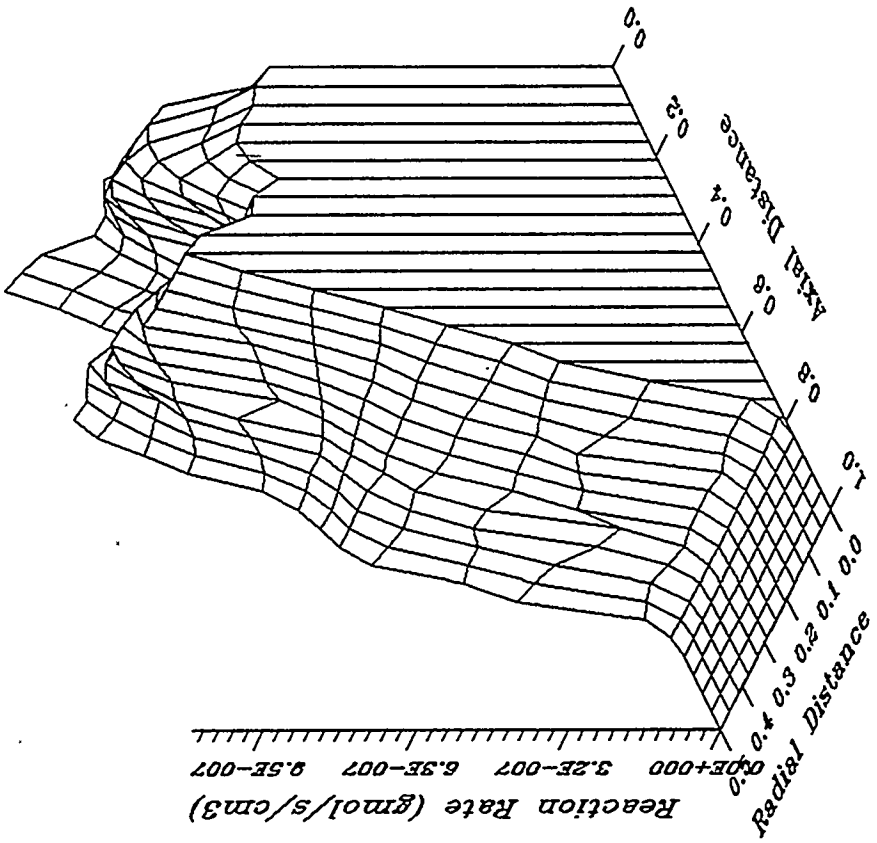

Figure 5.9 Instant Rate of Reaction (gmol/s/cm3)

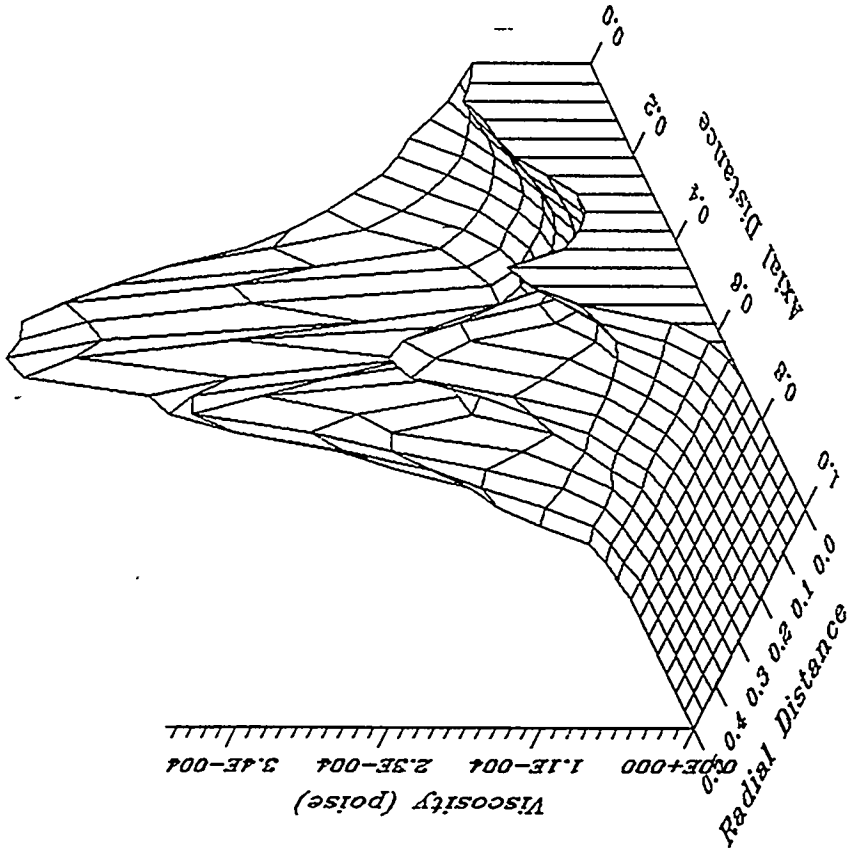

Figure 5.10 Solid Viscosity Distribution

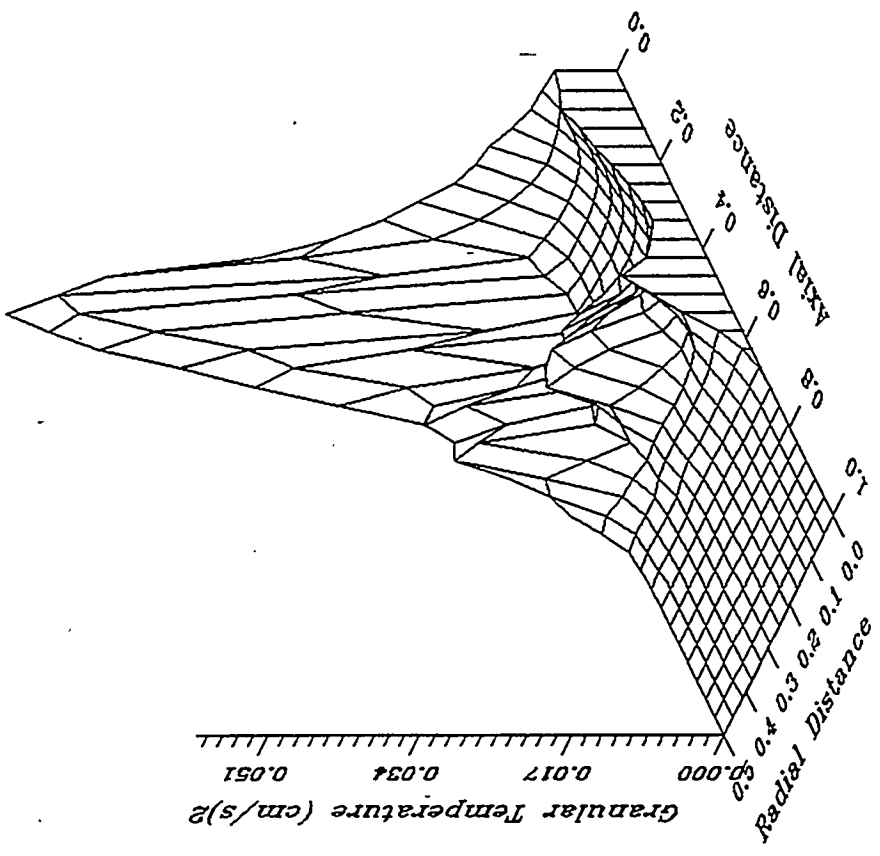

Figure 5.11 Solid Granular Temperature

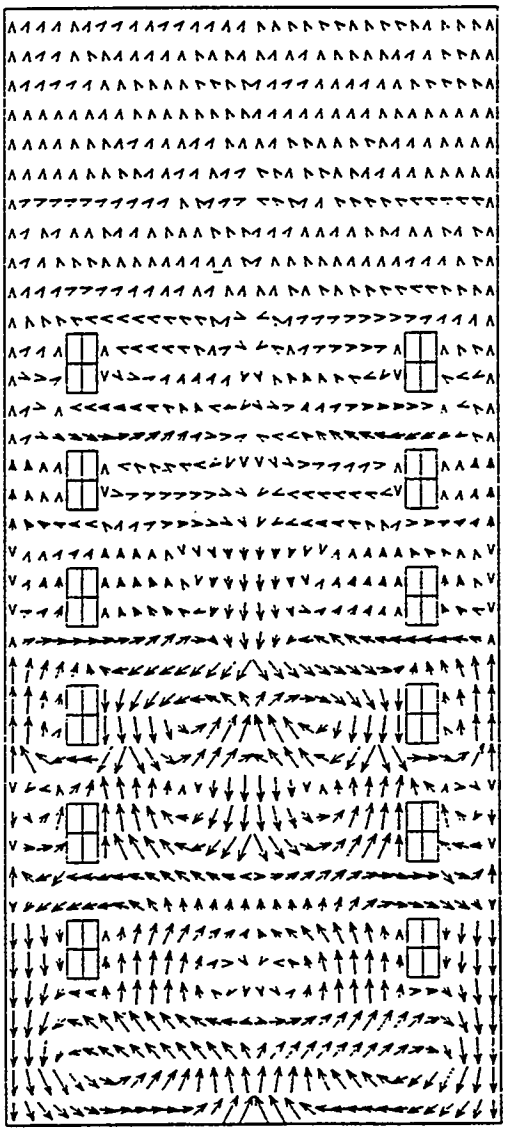

Figure 5.12 Gas Transient Flow Pattern

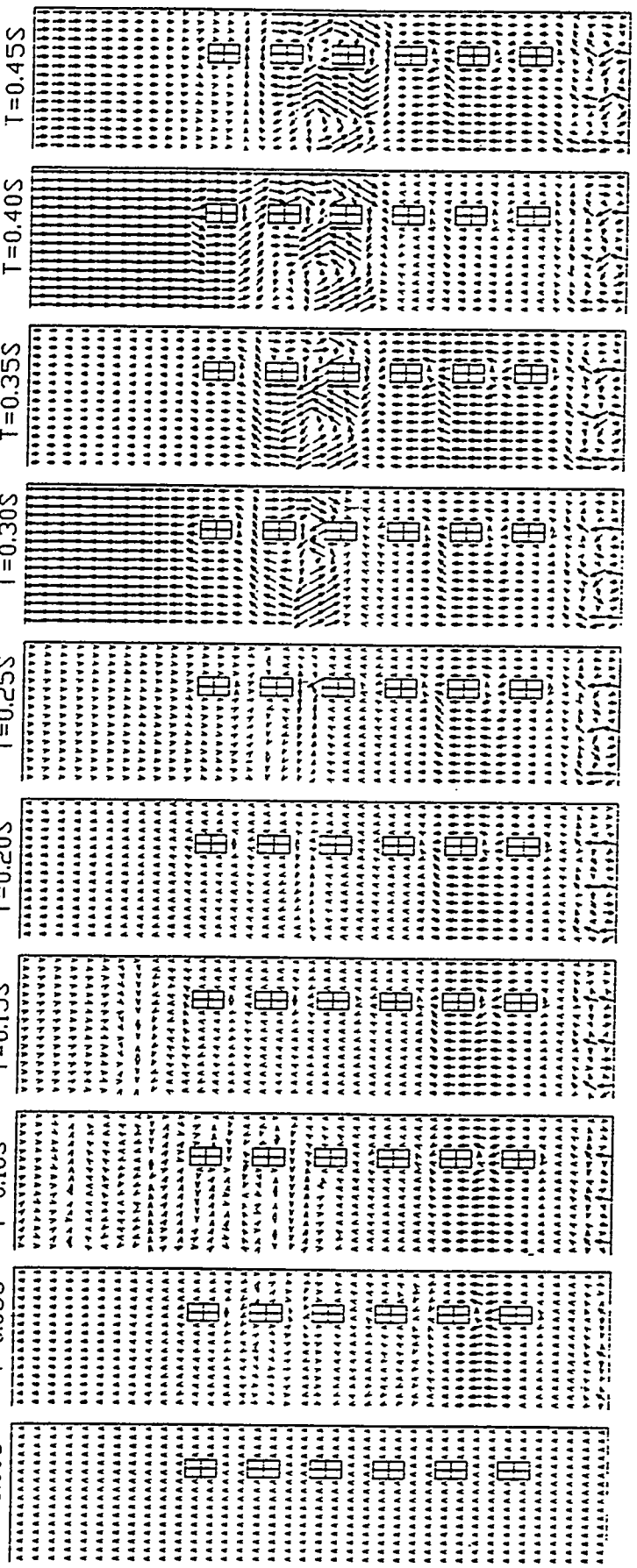

Figure 5.13 Time Series of Gas Flow Patterns

solutions. The finer the grid is, the more accurate the solution is. Under the limits of the computer speed and the capacity of storage, one can not choose an infinite fine grid. A reasonable grid needs to be chosen carefully without losing the accuracy and convergence of the solution. The usual way to check the convergence is to solve a problem with different grid size. To do so, a simulation run, based on the previous run for Air Products' reactor (Wu et al. 1995 and Pape et al. 1996), with fine grid was conducted using IIT's hydrodynamic code. The conditions of this run are exact same as the previous run except of the grid size, in which the dy of this run is one third less than that of the previous one.

Figure 5.14 shows the comparison of the time-averaged g-l-s volume fraction profiles in both runs. They have same slurry height, 530 cm. The curves of both runs demonstrate same profiles except of a minor difference.

Figure 5.15 and 5.16 show the frequency responses of the gas flowrate at the outlet. Both runs have approximately same frequency, 0.7 Hertz.

Figure 5.17 a&b and 5.18 a&b demonstrate the similar flow patterns in both runs that display down-flows at the walls, up-flow at the center and vortices near the bottom.

In summary, the computed slurry height, gas holdup and the rate of methanol production agree well with LaPorte's RUN E-8.1. The two-dimensional hydrodynamic model is better than the one-dimensional, steady state models in predicting the methanol production and hydrodynamics of slurry bubble column reactors.

Two grids are used in the simulations of the Air Products' reactor and a good agreement, indicating the accuracy and convergence of the simulations, is reached.

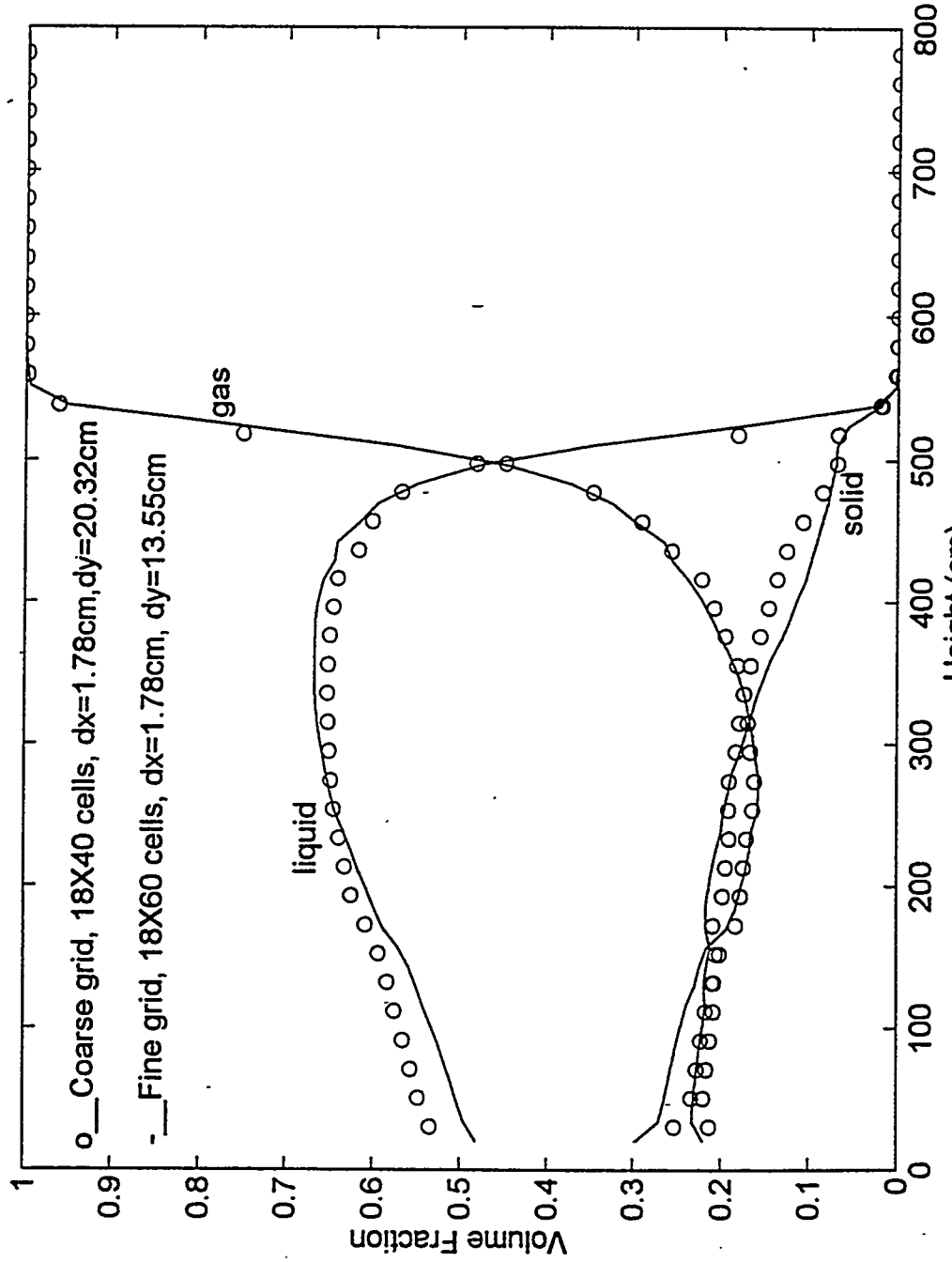

Figure 5.14 Time Average G-L-S Volume Fraction Profiles in Different Grid

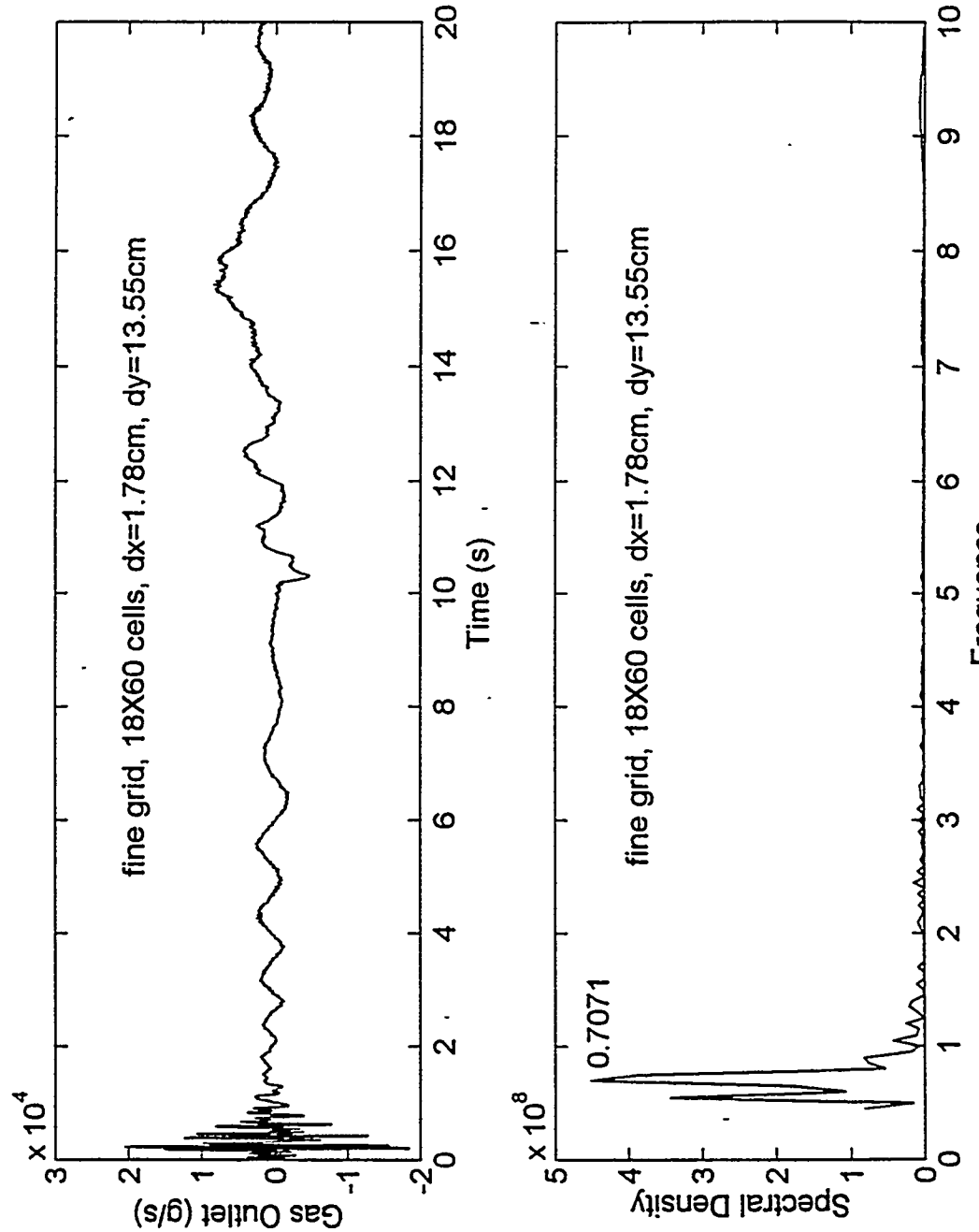

Figure 5.15 Gas Flowrate at Reactor Top and Frequence Response (Fine Grid)

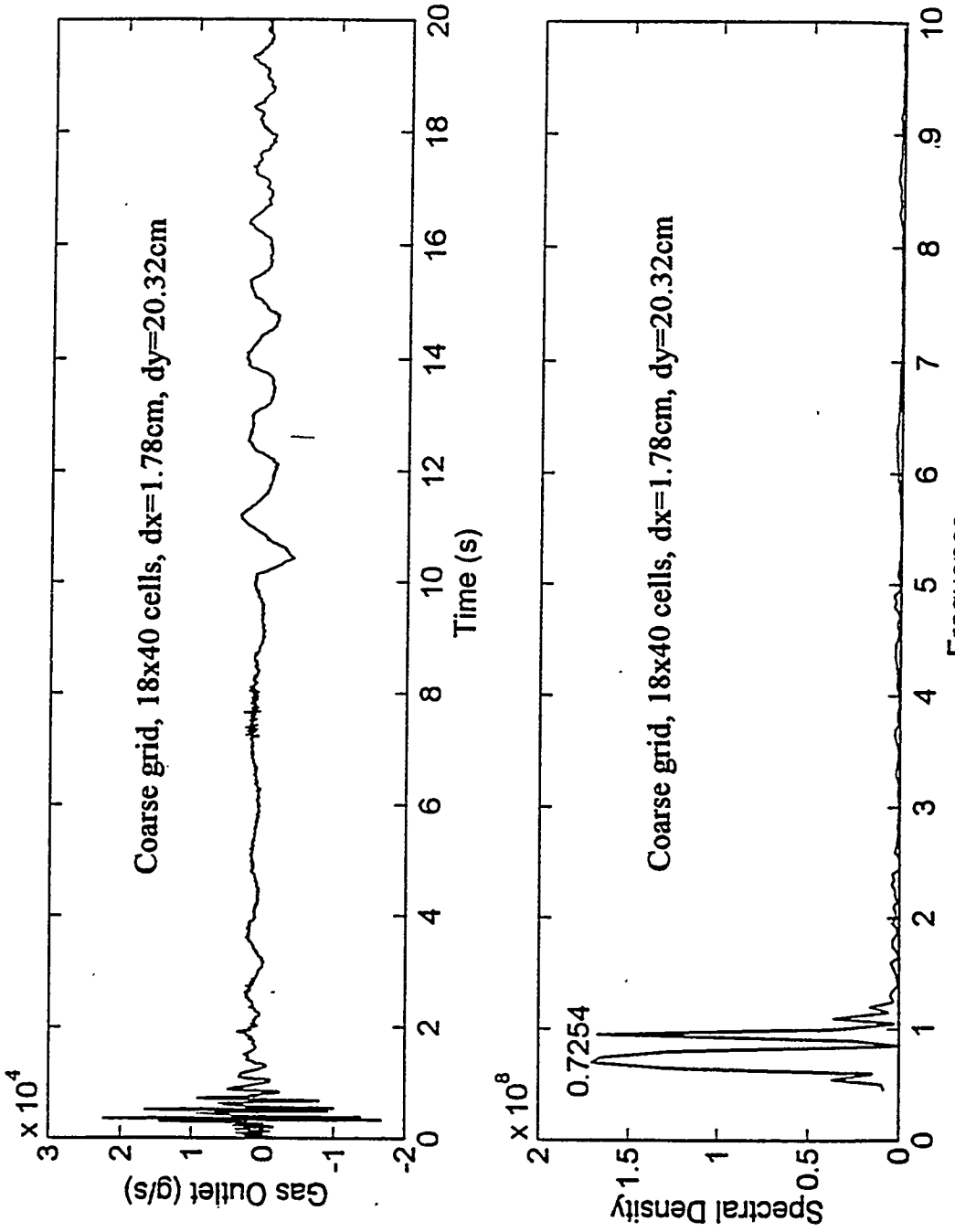

Figure 5.16 Gas Flowrate at Reactor Top and Frequence Response (Coarse Grid)

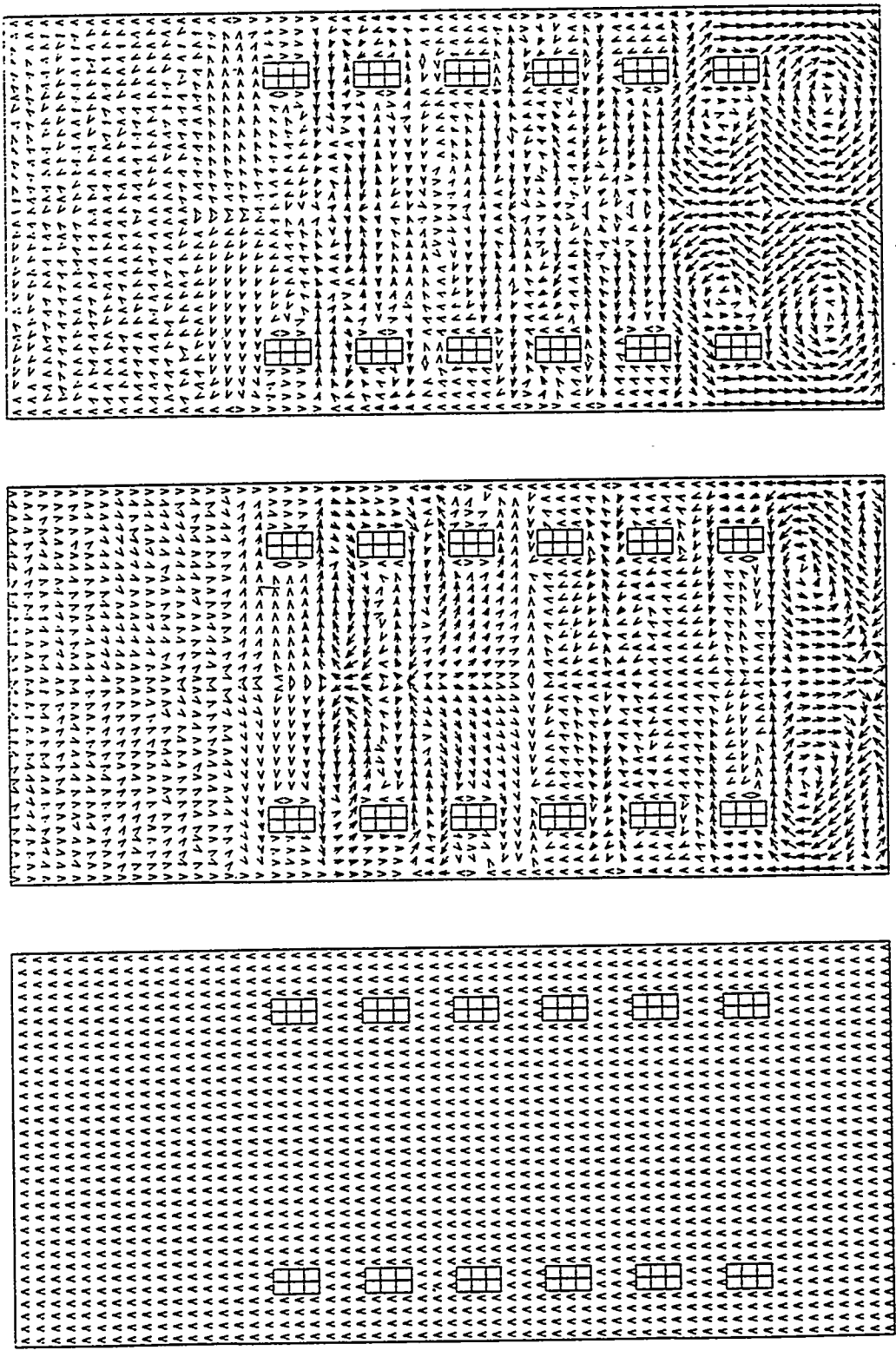

Figure 5.17a Gas Flow Patterns (Fine Grid)

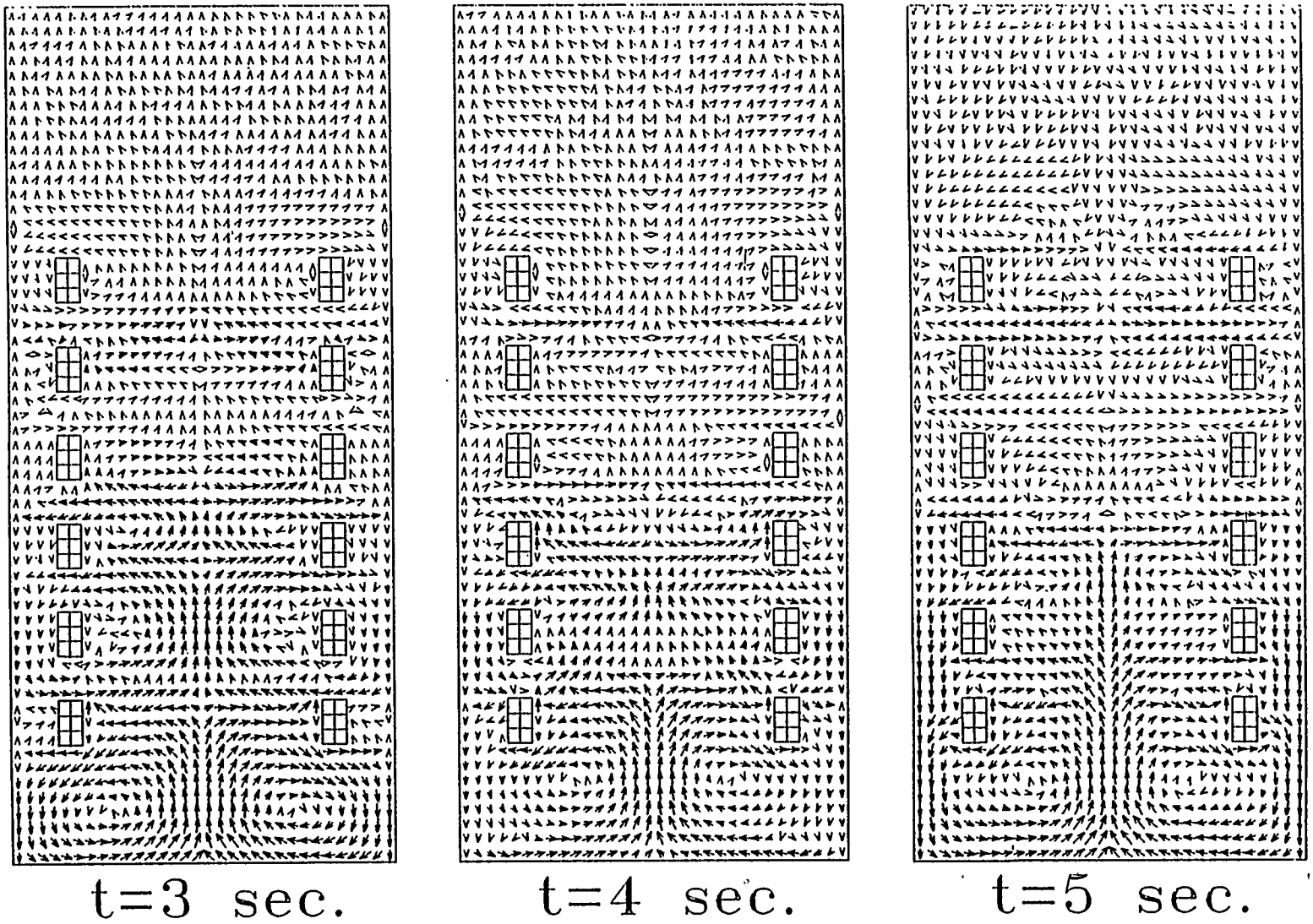

Figure 5.17b Gas Flow Patterns (Fine Grid)

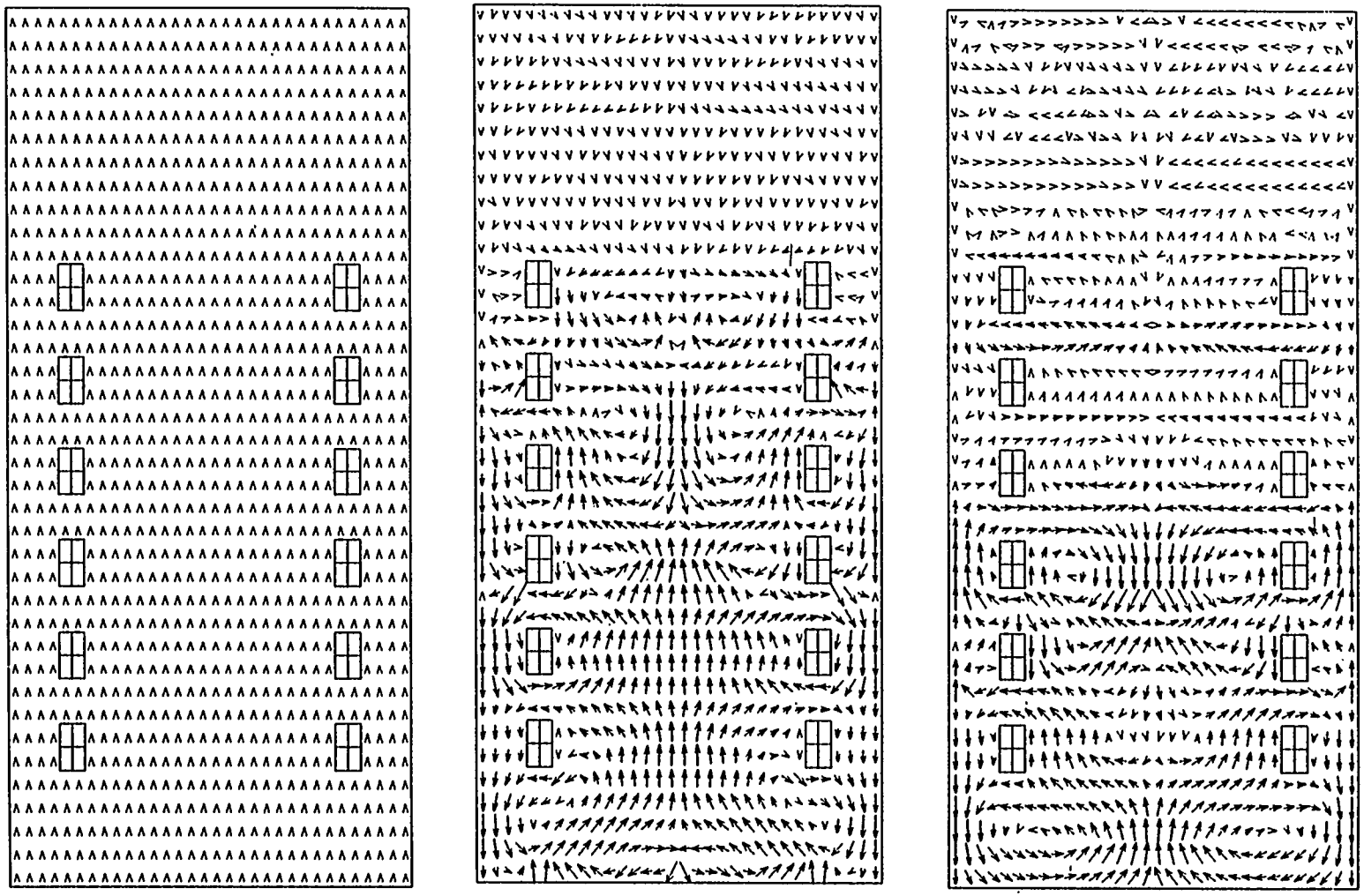

Figure 5.18a Gas Flow Patterns (Coarse Grid)

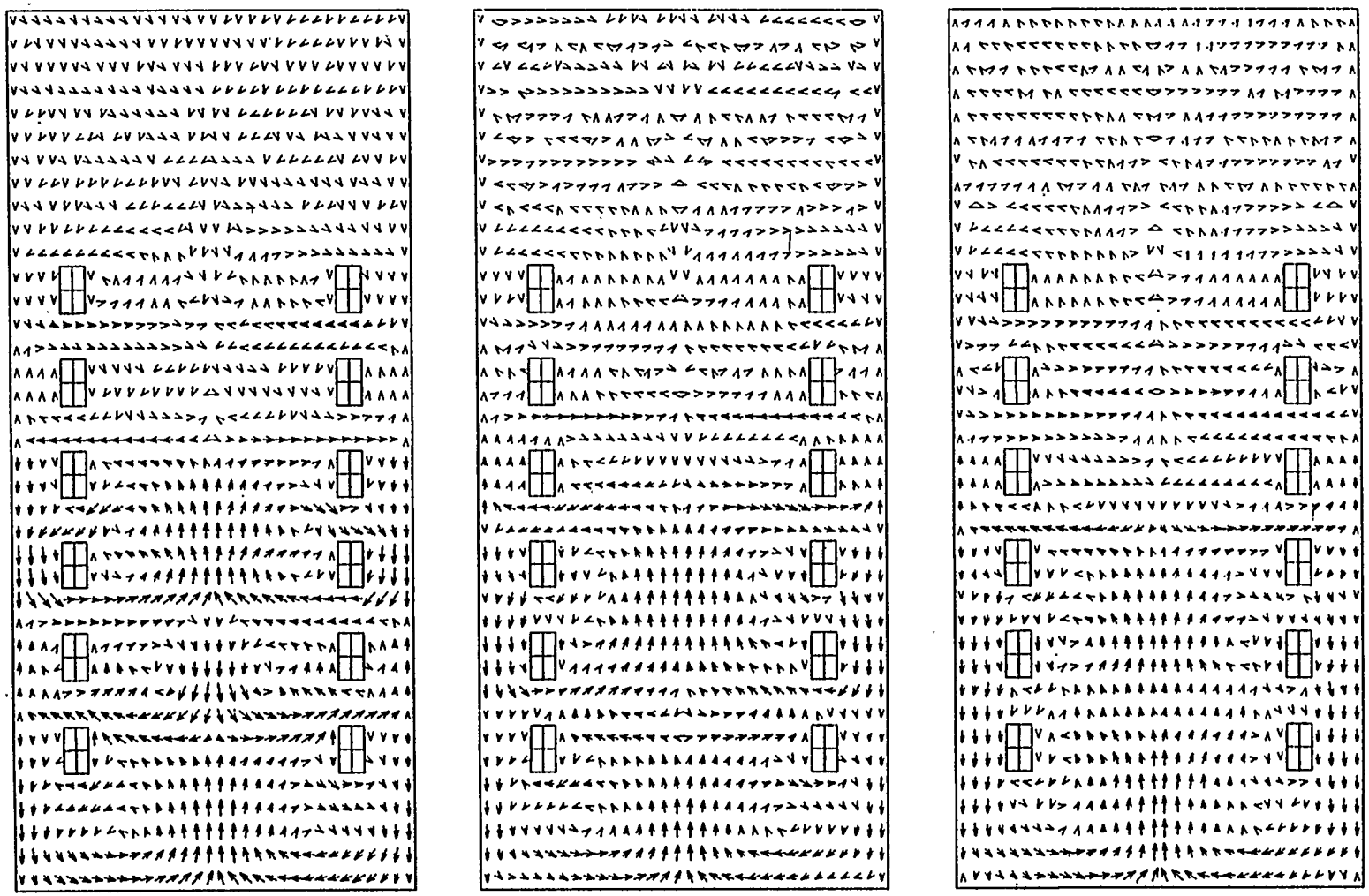

Figure 5.18b Gas Flow Patterns (Coarse Grid)